CHAPTER

6

POTENTIAL SWEEP METHODS

6.1 INTRODUCTION

The complete electrochemical behavior of a system can be obtained through a series of steps to different potentials with recording of the current-time curves, as described in Sections 5.4 and 5.5, to yield a three-dimensional *i-t-E* surface (Figure 6.1.1*a*). However, the accumulation and analysis of these data can be tedious especially when a stationary electrode is used. Also, it is not easy to recognize the presence of different species (i.e., to observe waves) from the recorded *i-t* curves alone, and potential steps that are very closely spaced (e.g., 1 mV apart) are needed for the derivation of well-resolved *i-E* curves. More information can be gained in a single experiment by sweeping the potential with time and recording the *i-E* curve directly. This amounts, in a qualitative way, to traversing the three-dimensional *i-t-E* realm (Figure 6.1.1*b*). Usually the potential is varied linearly with time (i.e., the applied signal is a voltage ramp) with sweep rates v ranging from 10 mV/s (1 V traversed in 100 s) to about 1000 V/s with conventional electrodes and up to 10^6 V/s with UMEs. In this experiment, it is customary to record the current as a function of potential, which is obviously equivalent to recording current versus time. The formal name for the method is *linear potential sweep chronoamperometry*, but most workers refer to it as *linear sweep voltammetry* (LSV).[1]

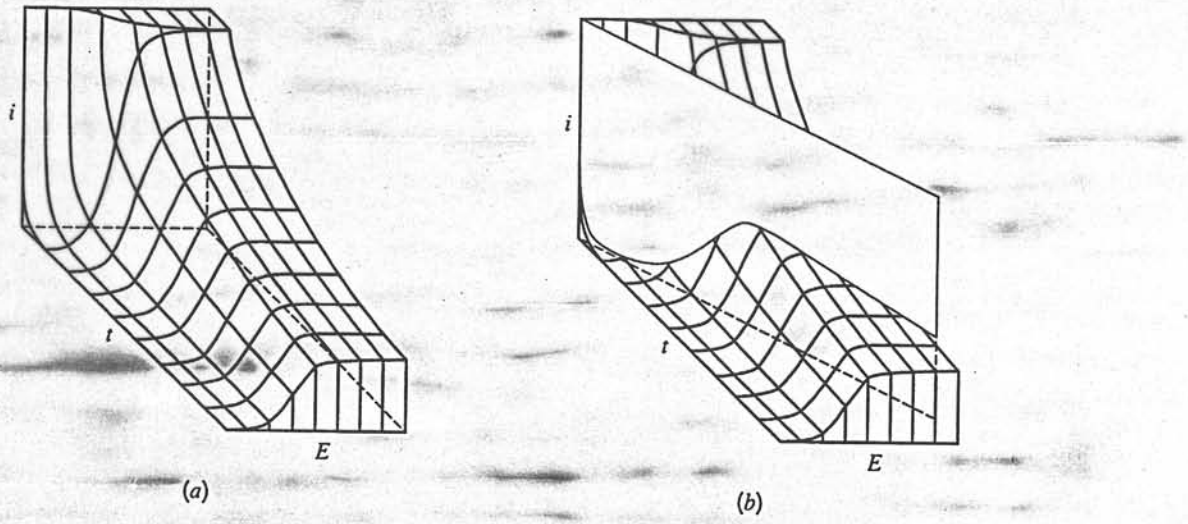

Figure 6.1.1 (*a*) A portion of the *i-t-E* surface for a nernstian reaction. Potential axis is in units of $60/n$ mV. (*b*) Linear potential sweep across this surface. [Reprinted with permission from W. H. Reinmuth, *Anal. Chem.*, **32**, 1509 (1960). Copyright 1960, American Chemical Society.]

[1]This method has also been called *stationary electrode polarography*; however, we will adhere to the recommended practice of reserving the term *polarography* for voltammetric measurements at the DME.

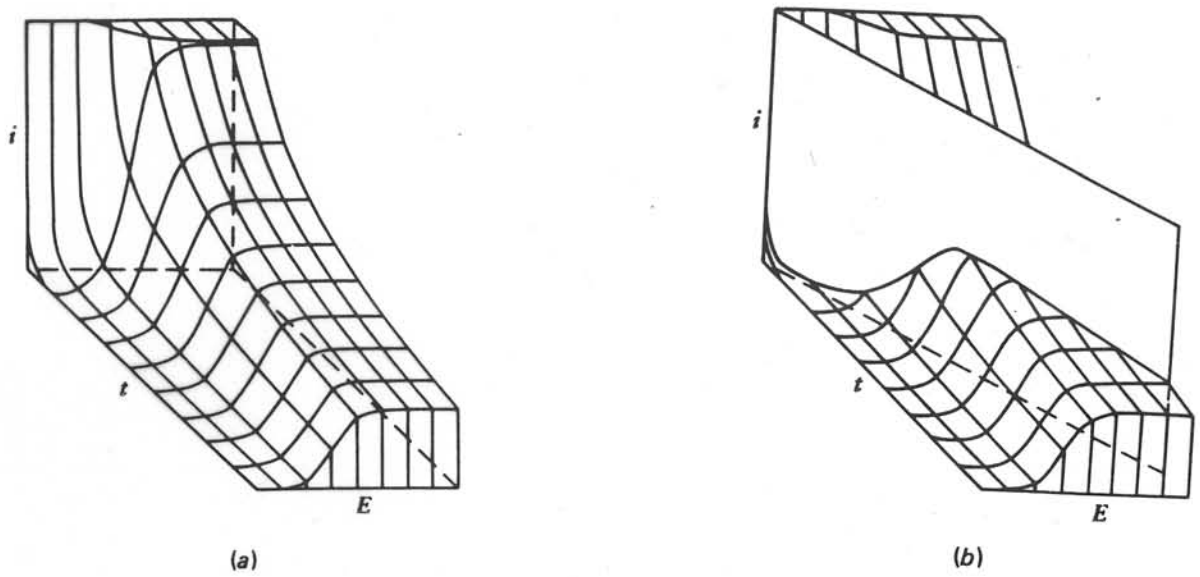

Figure 6.1.1

(*a*) Representation of a portion of the *i-t-E* surface for a nernstian reaction. Potential axis is in units of $60/n$ mV. (*b*) Linear potential sweep across this surface. [Reprinted with permission from W. H. Reinmuth, *Anal. Chem.*, **32**, 1509 (1960). Copyright 1960, American Chemical Society.]

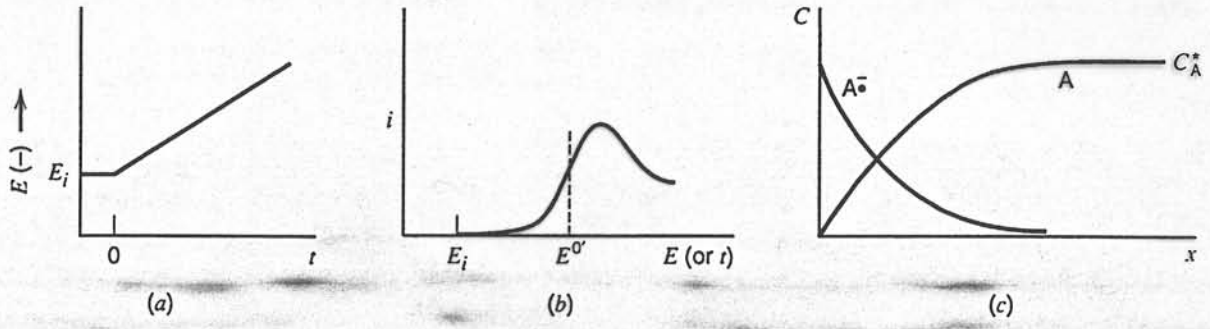

Figure 6.1.2 (*a*) Linear potential sweep or ramp starting at E_i. (*b*) Resulting *i*-*E* curve. (*c*) Concentration profiles of A and $A^{\bullet-}$ for potentials beyond the peak.

A typical LSV response curve for the anthracene system considered in Section 5.1 is shown in Figure 6.1.2*b*. If the scan is begun at a potential well positive of $E^{0'}$ for the reduction, only nonfaradaic currents flow for a while. When the electrode potential reaches the vicinity of $E^{0'}$ the reduction begins and current starts to flow. As the potential continues to grow more negative, the surface concentration of anthracene must drop; hence the flux to the surface (and the current) increases. As the potential moves past $E^{0'}$, the surface concentration drops nearly to zero, mass transfer of anthracene to the surface reaches a maximum rate, and then it declines as the depletion effect sets in. The observation is therefore a peaked current-potential curve like that depicted.

At this point, the concentration profiles near the electrode are like those shown in Figure 6.1.2*c*. Let us consider what happens if we reverse the potential scan (see Figure 6.1.3). Suddenly the potential is sweeping in a positive direction, and in the electrode's vicinity there is a large concentration of the oxidizable anion radical of anthracene. As the potential approaches, then passes, $E^{0'}$, the electrochemical balance at the surface grows more and more favorable toward the neutral anthracene species. Thus the anion radical becomes reoxidized and an anodic current flows. This reversal current has a shape much like that of the forward peak for essentially the same reasons.

This experiment, which is called *cyclic voltammetry* (CV), is a reversal technique and is the potential-scan equivalent of double potential step chronoamperometry (Section 5.7). Cyclic voltammetry has become a very popular technique for initial electrochemical studies of new systems and has proven very useful in obtaining information about fairly complicated electrode reactions. These will be discussed in more detail in Chapter 12.

In the next sections, we describe the solution of the diffusion equations with the appropriate boundary conditions for electrode reactions with heterogeneous rate constants spanning a wide range, and we discuss the observed responses. An analytical approach based on an integral equation is used here, because it has been widely applied to these types of problems and shows directly how the current is affected by different experimen-

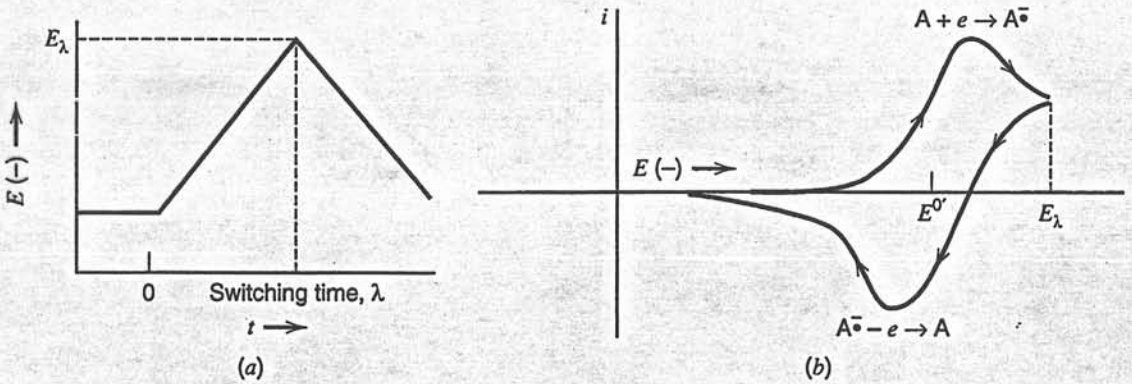

Figure 6.1.3 (*a*) Cyclic potential sweep. (*b*) Resulting cyclic voltammogram.

tal variables (e.g., scan rate and concentration). However, in most cases, particularly when the overall reactions are complicated by coupled homogeneous reactions (Chapter 12), digital simulation methods (Appendix B) are used to calculate voltammograms.

6.2 NERNSTIAN (REVERSIBLE) SYSTEMS

6.2.1 Solution of the Boundary Value Problem

We consider again the reaction $O + ne \rightleftarrows R$, assuming semi-infinite linear diffusion and a solution initially containing only species O, with the electrode held initially at a potential E_i, where no electrode reaction occurs. These initial conditions are identical to those in Section 5.4.1. The potential is swept linearly at v (V/s) so that the potential at any time is

$$E(t) = E_i - vt \tag{6.2.1}$$

If we can assume that the rate of electron transfer is rapid at the electrode surface, so that species O and R immediately adjust to the ratio dictated by the Nernst equation, then the equations of Section 5.4, that is, (5.4.2)–(5.4.6), still apply. However, (5.4.6) must be recognized as having a time-dependent form:

$$\frac{C_O(0,t)}{C_R(0,t)} = f(t) = \exp\left[\frac{nF}{RT}(E_i - vt - E^{0'})\right] \tag{6.2.2}$$

The time dependence is significant, because the Laplace transformation of (6.2.2) cannot be obtained as it could in deriving (5.4.13),[2] and the mathematics for sweep experiments are greatly complicated as a consequence. The problem was first considered by Randles (1) and Sevcik (2); the treatment and notation here follow the later work of Nicholson and Shain (3). The boundary condition (6.2.2) can be written

$$\frac{C_O(0,t)}{C_R(0,t)} = \theta e^{-\sigma t} = \theta S(t) \tag{6.2.3}$$

where $S(t) = e^{-\sigma t}$, $\theta = \exp[(nF/RT)(E_i - E^{0'})]$, and $\sigma = (nF/RT)v$. As before (see Section 5.4.1), Laplace transformation of the diffusion equations and application of the initial and semi-infinite conditions leads to [see (5.4.7)]

$$\bar{C}_O(x,s) = \frac{C_O^*}{s} + A(s)\exp\left[-\left(\frac{s}{D_O}\right)^{1/2} x\right] \tag{6.2.4}$$

The transform of the current is given by [see (5.2.9)]

$$\bar{i}(s) = nFAD_O\left[\frac{\partial \bar{C}_O(x,s)}{\partial x}\right]_{x=0} \tag{6.2.5}$$

Combining this with (6.2.4) and inverting, by making use of the convolution theorem (see Appendix A), we obtain[3]

$$C_O(0,t) = C_O^* - [nFA(\pi D_O)^{1/2}]^{-1}\int_0^t i(\tau)(t-\tau)^{-1/2}\,d\tau \tag{6.2.6}$$

[2]The Laplace transform of $C_O(0,t) = \theta C_R(0,t)$ is $\bar{C}_O(0,s) = \theta \bar{C}_R(0,s)$ only when θ is not a function of time; it is only under this condition that θ can be removed from the Laplace integral.

[3]This derivation is left as an exercise for the reader (see Problem 6.1). Equation 6.2.6 is often a useful starting point in other electrochemical treatments involving semi-infinite linear diffusion. τ in the integral is a dummy variable that is lost when the definite integral is evaluated.

By letting

$$f(\tau) = \frac{i(\tau)}{nFA} \tag{6.2.7}$$

(6.2.6) can be written

$$\boxed{C_O(0, t) = C_O^* - (\pi D_O)^{-1/2} \int_0^t f(\tau)(t - \tau)^{-1/2}\, d\tau} \tag{6.2.8}$$

Similarly from (5.4.12) an expression for $C_R(0, t)$can be obtained (assuming R is initially absent):

$$\boxed{C_R(0, t) = (\pi D_R)^{-1/2} \int_0^t f(\tau)(t - \tau)^{-1/2}\, d\tau} \tag{6.2.9}$$

The derivation of (6.2.8) and (6.2.9) employed only the linear diffusion equations, initial conditions, semi-infinite conditions, and the flux balance. No assumption related to electrode kinetics or technique was made; hence (6.2.8) and (6.2.9) are general. From these equations and the boundary condition for LSV, (6.2.3), we obtain

$$\int_0^t f(\tau)(t - \tau)^{-1/2}\, d\tau = \frac{C_O^*}{[\theta S(t)(\pi D_R)^{-1/2} + (\pi D_O)^{-1/2}]} \tag{6.2.10}$$

$$\int_0^t i(\tau)(t - \tau)^{-1/2}\, d\tau = \frac{nFA\pi^{1/2} D_O^{1/2} C_O^*}{[\theta S(t)\xi + 1]} \tag{6.2.11}$$

where, as before, $\xi = (D_O/D_R)^{1/2}$. The solution of this last integral equation would be the function $i(t)$, embodying the desired current-time curve, or, since potential is linearly related to time, the current-potential equation. A closed-form solution of (6.2.11) cannot be obtained, and a numerical method must be employed.

Before solving (6.2.11) numerically, it is convenient (a) to change from $i(t)$ to $i(E)$, since that is the way in which the data are usually considered, and (b) to put the equation in a dimensionless form so that a single numerical solution will give results that will be useful under any experimental conditions. This is accomplished by using the following substitution:

$$\sigma t = \frac{nF}{RT} vt = \left(\frac{nF}{RT}\right)(E_i - E) \tag{6.2.12}$$

Let $f(\tau) = g(\sigma\tau)$. With $z = \sigma\tau$, so that $\tau = z/\sigma$, $d\tau = dz/\sigma$, $z = 0$ at $\tau = 0$, and $z = \sigma t$ at $\tau = t$, we obtain

$$\int_0^t f(\tau)(t - \tau)^{-1/2}\, d\tau = \int_0^{\sigma t} g(z)\left(t - \frac{z}{\sigma}\right)^{-1/2} \frac{dz}{\sigma} \tag{6.2.13}$$

so that (6.2.11) can be written

$$\int_0^{\sigma t} g(z)(\sigma t - z)^{-1/2}\, \sigma^{-1/2}\, dz = \frac{C_O^*(\pi D_O)^{1/2}}{1 + \xi\theta S(\sigma t)} \tag{6.2.14}$$

or finally, dividing by $C_O^*(\pi D_O)^{1/2}$, we obtain

$$\int_0^{\sigma t} \frac{\chi(z)\, dz}{(\sigma t - z)^{1/2}} = \frac{1}{1 + \xi\theta S(\sigma t)} \tag{6.2.15}$$

where

$$\chi(z) = \frac{g(z)}{C_O^*(\pi D_O \sigma)^{1/2}} = \frac{i(\sigma t)}{nFAC_O^*(\pi D_O \sigma)^{1/2}} \tag{6.2.16}$$

Note that (6.2.15) is the desired equation in terms of the dimensionless variables $\chi(z)$, ξ, θ, $S(\sigma t)$ and σt. Thus at any value of $S(\sigma t)$, which is a function of E, $\chi(\sigma t)$ can be obtained by solution of (6.2.15) and, from it, the current can be obtained by rearrangement of (6.2.16):

$$i = nFAC_O^*(\pi D_O \sigma)^{1/2}\,\chi(\sigma t) \tag{6.2.17}$$

At any given point, $\chi(\sigma t)$ is a pure number, so that (6.2.17) gives the functional relationship between the current at any point on the LSV curve and the variables. Specifically, i is proportional to C_O^* and $v^{1/2}$. The solution of (6.2.15) has been carried out numerically [Nicholson and Shain (3)], by a series solution [Sevcik (2), Reinmuth (4)], analytically in terms of an integral that must be evaluated numerically [Matsuda and Ayabe (5), Gokhshtein (6)], and by related methods (7, 8). The general result of solving (6.2.15) is a set of values of $\chi(\sigma t)$ (see Table 6.2.1 and Figure 6.2.1) as a function of σt or $n(E - E_{1/2})$.[4]

TABLE 6.2.1 Current Functions for Reversible Charge Transfer (3)[a,b]

$\frac{n(E-E_{1/2})}{RT/F}$	$n(E-E_{1/2})$ mV at 25°C	$\pi^{1/2}\chi(\sigma t)$	$\phi(\sigma t)$	$\frac{n(E-E_{1/2})}{RT/F}$	$n(E-E_{1/2})$ mV at 25°C	$\pi^{1/2}\chi(\sigma t)$	$\phi(\sigma t)$
4.67	120	0.009	0.008	−0.19	−5	0.400	0.548
3.89	100	0.020	0.019	−0.39	−10	0.418	0.596
3.11	80	0.042	0.041	−0.58	−15	0.432	0.641
2.34	60	0.084	0.087	−0.78	−20	0.441	0.685
1.95	50	0.117	0.124	−0.97	−25	0.445	0.725
1.75	45	0.138	0.146	−1.109	−28.50	0.4463	0.7516
1.56	40	0.160	0.173	−1.17	−30	0.446	0.763
1.36	35	0.185	0.208	−1.36	−35	0.443	0.796
1.17	30	0.211	0.236	−1.56	−40	0.438	0.826
0.97	25	0.240	0.273	−1.95	−50	0.421	0.875
0.78	20	0.269	0.314	−2.34	−60	0.399	0.912
0.58	15	0.298	0.357	−3.11	−80	0.353	0.957
0.39	10	0.328	0.403	−3.89	−100	0.312	0.980
0.19	5	0.355	0.451	−4.67	−120	0.280	0.991
0.00	0	0.380	0.499	−5.84	−150	0.245	0.997

[a] To calculate the current:

1. $i = i$(plane) + i(spherical correction).
2. $i = nFAD_O^{1/2}C_O^*\sigma^{1/2}\pi^{1/2}\chi(\sigma t) + nFAD_O C_O^*(1/r_0)\phi(\sigma t)$.
3. $i = 602n^{3/2}AD_O^{1/2}C_O^* v^{1/2}\{\pi^{1/2}\chi(\sigma t) + 0.160[D_O^{1/2}/(r_O n^{1/2} v^{1/2})]\phi(\sigma t)\}$ at 25°C with quantities in the following units: i, amperes; A, cm^2; D_O, cm^2/s; v, V/s; C_O^*, M; r_0, cm.

[b] $E_{1/2} = E^{0'} + (RT/nF)\ln(D_R/D_O)^{1/2}$.

[4] Note that $\ln \xi\theta S(\sigma t) = nf(E - E_{1/2})$, where $E_{1/2} \equiv E^{0'} + (RT/nF)\ln(D_R/D_O)^{1/2}$.

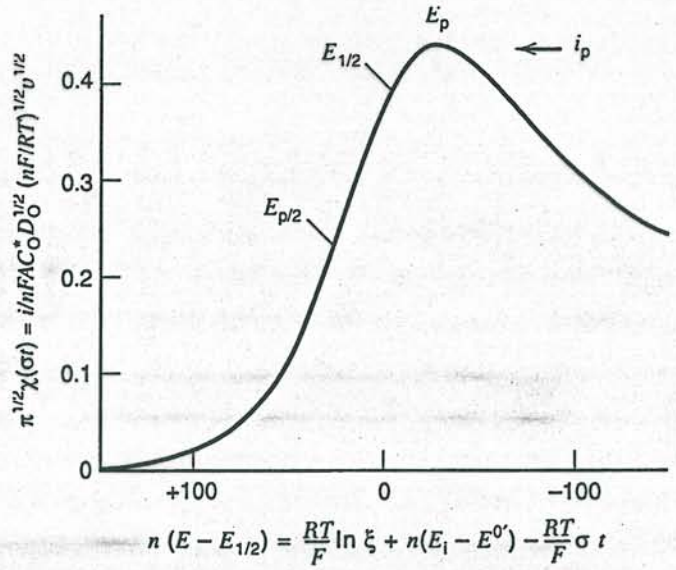

Figure 6.2.1 Linear potential sweep voltammogram in terms of dimensionless current function. Values on the potential axis are for 25°C

6.2.2 Peak Current and Potential

The function $\pi^{1/2}\chi(\sigma t)$, and hence the current, reaches a maximum where $\pi^{1/2}\chi(\sigma t) = 0.4463$. From (6.2.17) the *peak current*, i_p, is

$$i_p = 0.4463\left(\frac{F^3}{RT}\right)^{1/2} n^{3/2} A D_O^{1/2} C_O^* v^{1/2} \tag{6.2.18}$$

At 25°C, for A in cm^2, D_O in cm^2/s, C_O^* in mol/cm^3, and v in V/s, i_p in amperes is

$$i_p = (2.69 \times 10^5) n^{3/2} A D_O^{1/2} C_O^* v^{1/2} \tag{6.2.19}$$

The *peak potential*, E_p, is found from Table 6.2.1 to be

$$E_p = E_{1/2} - 1.109\frac{RT}{nF} = 28.5/n \text{ mV at } 25°C \tag{6.2.20}$$

Because the peak is somewhat broad, so that the peak potential may be difficult to determine, it is sometimes convenient to report the potential at $i_p/2$, called the *half-peak potential*, $E_{p/2}$, which is

$$E_{p/2} = E_{1/2} + 1.09\frac{RT}{nF} = E_{1/2} + 28.0/n \text{ mV at } 25°C \tag{6.2.21}$$

Note that $E_{1/2}$ is located just about midway between E_p and $E_{p/2}$, and that a convenient diagnostic for a nernstian wave is

$$|E_p - E_{p/2}| = 2.20\frac{RT}{nF} = 56.5/n \text{ mV at } 25°C \tag{6.2.22}$$

Thus for a reversible wave, E_p is independent of scan rate, and i_p (as well as the current at any other point on the wave) is proportional to $v^{1/2}$. The latter property indicates diffusion control and is analogous to the variation of i_d with $t^{-1/2}$ in chronoamperometry. A convenient constant in LSV is $i_p/v^{1/2}C_O^*$ (sometimes called the *current function*), which depends on $n^{3/2}$ and $D_O^{1/2}$. This constant can be used to estimate n for an electrode

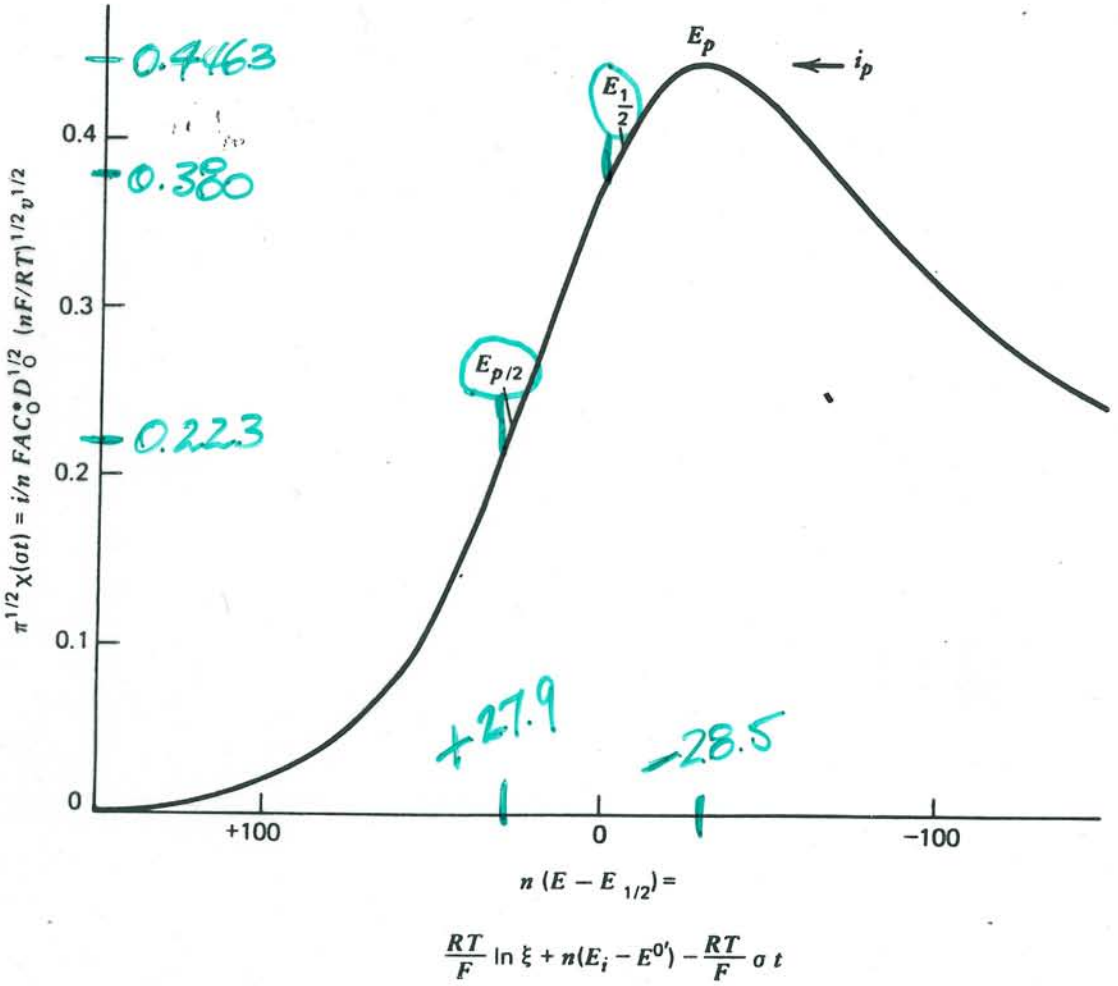

Figure 6.2.1
Linear potential sweep voltammogram in terms of dimensionless current function.

i	E	$\pi^{1/2}\chi(\sigma t)$	$(E - E_{1/2})n$
i_p	E_p	0.4463	−28.50
$i_p/2$	$E_{p/2}$	0.223	+27.9
$0.851\,i_p$	$E_{1/2}$	0.380	0

reaction, if a value of D_O can be estimated, for example, from the LSV of a compound of similar size or structure that undergoes an electrode reaction with a known n value.

6.2.3 Spherical Electrodes and UMEs

For LSV with a spherical electrode (e.g., a hanging mercury drop), a similar treatment can be presented (4); the resulting current is

$$i = i(\text{plane}) + \frac{nFAD_O C_O^* \phi(\sigma t)}{r_0} \tag{6.2.23}$$

where r_0 is the radius of the electrode and $\phi(\sigma t)$ is a tabulated function (see Table 6.2.1). For large values of v and with electrodes of conventional size the i (plane) term is much larger than the spherical correction term, and the electrode can be considered planar under these conditions.

Basically, the same considerations apply to hemispherical and ultramicroelectrodes at fast scan rates. However, for a UME, where r_0 is small, the second term will dominate at sufficiently small scan rates. One can show from (6.2.23) that this is true when

$$v << RTD/nFr_0^2 \tag{6.2.24}$$

so that the voltammogram will be a steady-state response independent of v.[5] For $r_0 = 5\ \mu$m, $D = 10^{-5}$ cm^2/s, and $T = 298$ K, the right side of (6.2.24) has a value of 1000 mV/s; thus a scan made at ~100 mV/s or slower should permit the accurate recording of steady-state currents. The limit depends on the square of the radius, so it is generally impractical to record steady-state voltammograms with electrodes much larger than those normally considered to be UMEs. Conversely, with very small UMEs, one requires a high sweep rate to see any behavior other than the steady state. For example, at an electrode of 0.5-μm radius and with D and T as given above, steady-state behavior would hold up to 10 V/s.

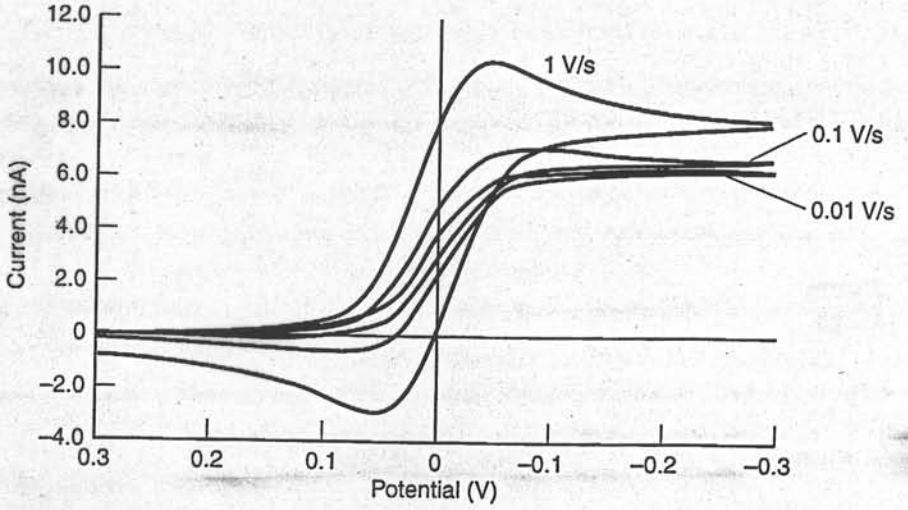

Figure 6.2.2 Effect of scan rate on cyclic voltammograms for an ultramicroelectrode (hemispherical diffusion) with 10 μm radius. Simulations for a nernstian reaction with $n = 1$, $E^{0'} = 0.0$ V, $D_O = D_R = 1 \times 10^{-5}$ cm^2/s, $C_O^* = 1.0$ mM, and $T = 25$°C. At 1 V/s, the response begins to show the peak expected for linear diffusion, but the height of the current at the switching potential and the small peak current ratio show that the steady-state component is still dominant.

[5]Relationship 6.2.24 involves a comparison of a diffusion length to the radius of the electrode in the manner discussed in Section 5.2.2. The diffusion length is $[D_O/(nfv)]^{1/2}$, which corresponds to the time $1/(nfv)$. This is the period required for the scan to cover an energy ϵT along the potential axis (25.7/n mV at 25°C). It is often regarded as the characteristic time of an LSV or CV experiment (Chapter 12).

The transition from typical peak-shaped voltammograms at fast sweep rates in the linear diffusion region to steady-state voltammograms at small v is shown for cyclic voltammetry in Figure 6.2.2. In the steady-state region, the voltammograms are S-shaped and follow the treatment in Sections 1.4.2 and 5.4.2. Ultramicroelectrodes are almost always employed in the limiting regions: the linear region when $v^{1/2}/r_0$ is large and the steady-state region when $v^{1/2}/r_0$ is small. There is nothing additional to be gained from working in the mathematically more complicated intermediate region.

6.2.4 Effect of Double-Layer Capacitance and Uncompensated Resistance

For a potential step experiment at a stationary, constant-area electrode, the charging current dies away after a time equivalent to a few time constants (R_uC_d) (see Section 1.2.4). Since the potential is continuously changing in a potential sweep experiment, a charging current, i_c, always flows (see equation 1.2.15):

$$|i_c| = AC_d v \tag{6.2.25}$$

and the faradaic current must always be measured from a baseline of charging current (Figure 6.2.3). While i_p varies with $v^{1/2}$ for linear diffusion, i_c varies with v, so that i_c becomes relatively more important at faster scan rates. From (6.2.19) and (6.2.25)

$$\frac{|i_c|}{i_p} = \frac{C_d v^{1/2}(10^{-5})}{2.69n^{3/2}D_O^{1/2}C_O^*} \tag{6.2.26}$$

or for $D_O = 10^{-5}$cm^2/s and C_d= 20 μF/cm^2,

$$\frac{|i_c|}{i_p} \approx \frac{(2.4 \times 10^{-8})v^{1/2}}{n^{3/2}C_O^*} \tag{6.2.27}$$

Thus at high v and low C_O^* values, severe distortion of the LSV wave occurs. This effect often sets the limits of maximum useful scan rate and minimum useful concentration.

In general, a potentiostat controls $E + iR_u$, rather than the true potential of the working electrode (Sections 1.3.4 and 15.6.1). Since i varies with time as the peak is traversed, the error in potential varies correspondingly. If i_pR_u is appreciable compared to the accuracy of measurement (e.g., a few mV), the sweep will not be truly linear and the condition given by (6.2.1) does not hold. Moreover, the time required for the current to rise to the level given in (6.2.25) depends upon the electrode time constant, R_uC_d, as shown in (1.2.15). The practical effect of R_u is to flatten the wave and to shift the reduction peak toward more negative potentials. Since the current increases with $v^{1/2}$, the larger the scan rate, the more E_p will be shifted, so that appreciable R_u causes E_p to be a function of v. It moves systematically in a negative direction with increasing v (for a reduction). Uncompensated resistance can thus have the insidious effect of mimicking the response found with heterogeneous kinetic limitations (as discussed in Sections 6.3 and 6.4).

By using a UME, one can extend the useful range of sweep rates to the 10^6 V/s region. Because the measured currents at the UME are small, the iR_u drop does not perturb the response or the applied excitation to the same extent as with larger electrodes. The much smaller R_uC_d at the UME also leads to less distortion in the voltammogram. However, even with the UME (6.2.27) applies, so the faradaic wave lies on top of a large capacitive current. To extract the desired information from the voltammogram, the total response (capacitive plus faradaic) can be simulated (9) or perturbations caused by C_d and R_u can be subtracted (10). Alternatively, positive feedback circuitry with a fast response can be used to compensate for distortions otherwise caused by R_u (11).

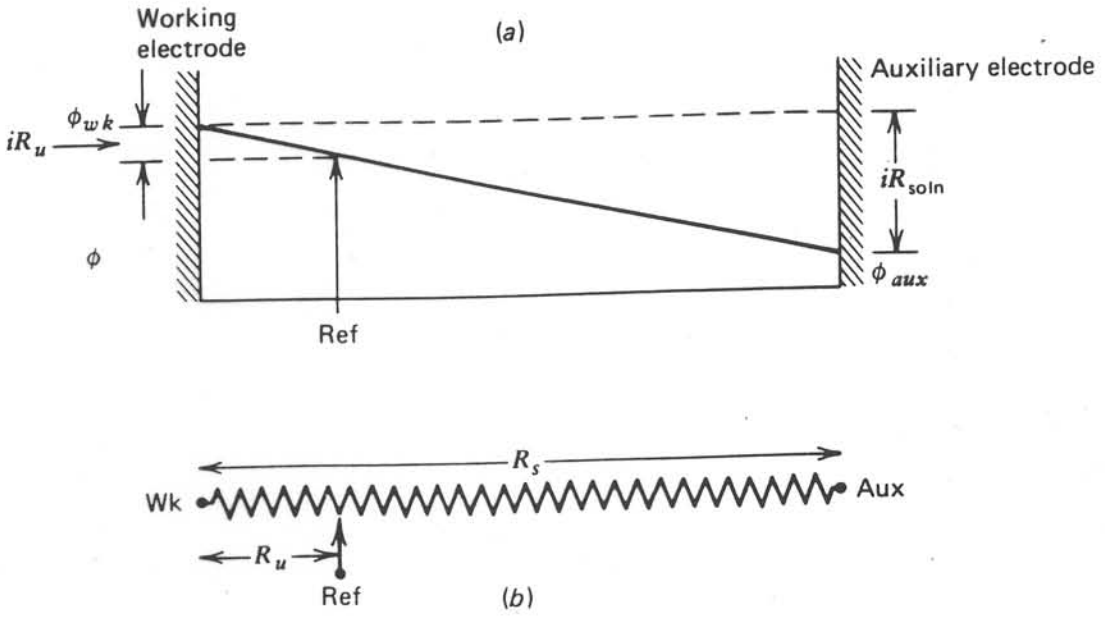

Figure 1.3.12

(*a*) Potential drop between working and auxiliary electrodes in solution and iR_u measured at reference electrode. (*b*) Representation of the cell as a potentiometer.

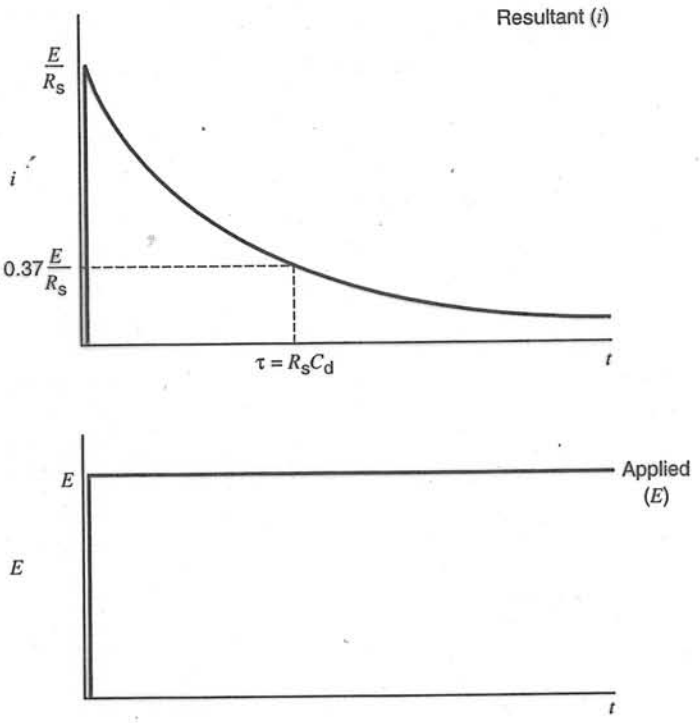

Figure 1.2.7 Current transient (*i vs. t*) resulting from a potential step experiment.

(b) Current Step

When the R_sC_d circuit is charged by a constant current (Figure 1.2.8), then equation 1.2.8 again applies. Since $q = \int i dt$, and i is a constant,

$$E = iR_s + \frac{i}{C_d}\int_0^t dt \tag{1.2.11}$$

or

$$\boxed{E = i(R_s + t/C_d)} \tag{1.2.12}$$

Hence, the potential increases linearly with time for a current step (Figure 1.2.9).

(c) Voltage Ramp (or Potential Sweep)

A *voltage ramp* or *linear potential sweep* is a potential that increases linearly with time starting at some initial value (here assumed to be zero) at a sweep rate v (in V s^{-1}) (see Figure 1.2.10*a*).

$$E = vt \tag{1.2.13}$$

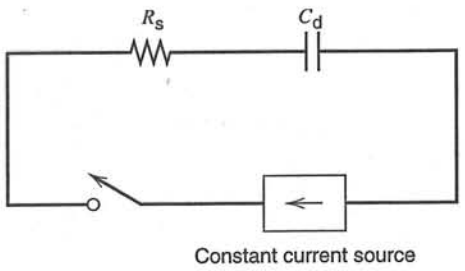

Figure 1.2.8 Current step experiment for an *RC* circuit.

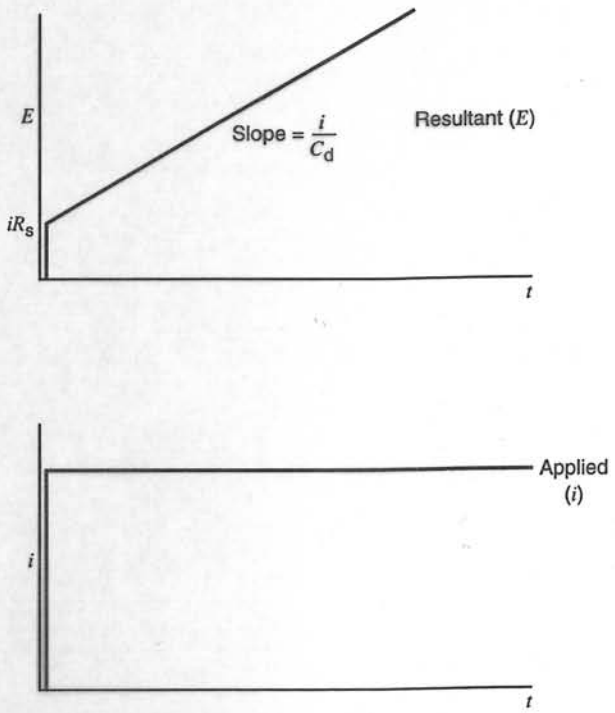

Figure 1.2.9 *E-t* behavior resulting from a current step experiment.

If such a ramp is applied to the R_sC_d circuit, equation 1.2.8 still applies; hence

$$vt = R_s(dq/dt) + q/C_d \tag{1.2.14}$$

If $q = 0$ at $t = 0$,

$$i = vC_d\,[1 - \exp(-t/R_sC_d)] \tag{1.2.15}$$

The current rises from zero as the scan starts and attains a steady-state value, vC_d (Figure 1.2.10*b*). This steady-state current can then be used to estimate C_d. If the time constant,

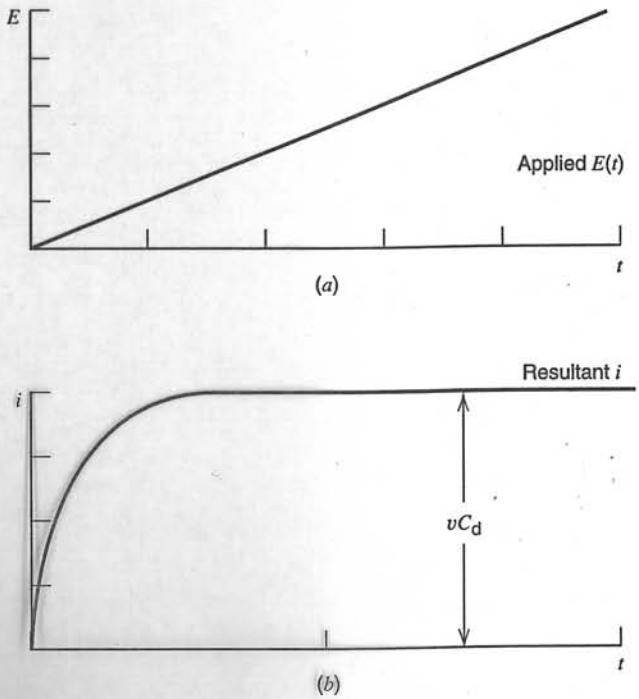

Figure 1.2.10 Current-time behavior resulting from a linear potential sweep applied to an *RC* circuit.

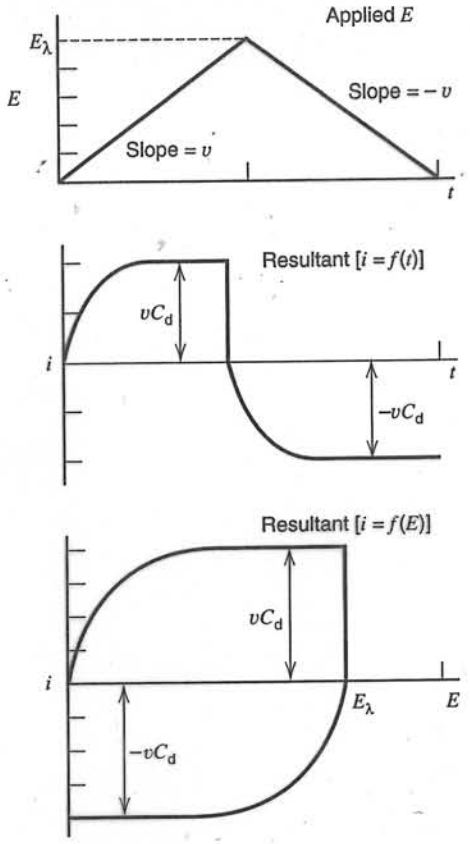

Figure 1.2.11 Current-time and current-potential plots resulting from a cyclic linear potential sweep (or triangular wave) applied to an *RC* circuit.

R_sC_d, is small compared to v, the instantaneous current can be used to measure C_d as a function of E.

If one instead applies a *triangular wave* (i.e., a ramp whose sweep rate switches from v to $-v$ at some potential, E_λ), then the steady-state current changes from vC_d during the forward (increasing E) scan to $-vC_d$ during the reverse (decreasing E) scan. The result for a system with constant C_d is shown in Figure 1.2.11.

▶ 1.3 FARADAIC PROCESSES AND FACTORS AFFECTING RATES OF ELECTRODE REACTIONS

1.3.1 Electrochemical Cells—Types and Definitions

Electrochemical cells in which faradaic currents are flowing are classified as either *galvanic* or *electrolytic* cells. A *galvanic cell* is one in which reactions occur spontaneously at the electrodes when they are connected externally by a conductor (Figure 1.3.1*a*). These cells are often employed in converting chemical energy into electrical energy. Galvanic cells of commercial importance include *primary* (*nonrechargeable*) *cells* (e.g., the Leclanché Zn–MnO_2 cell), *secondary* (*rechargeable*) *cells* (e.g., a charged Pb–PbO_2 storage battery), and *fuel cells* (e.g., an H_2–O_2 cell). An *electrolytic cell* is one in which reactions are effected by the imposition of an external voltage greater than the open-circuit potential of the cell (Figure 1.3.1*b*). These cells are frequently employed to carry out desired chemical reactions by expending electrical energy. Commercial processes involving electrolytic cells include electrolytic syntheses (e.g., the production of chlorine and aluminum), electrorefining (e.g., copper), and electroplating (e.g., silver and gold). The lead–acid storage cell, when it is being "recharged," is an electrolytic cell.

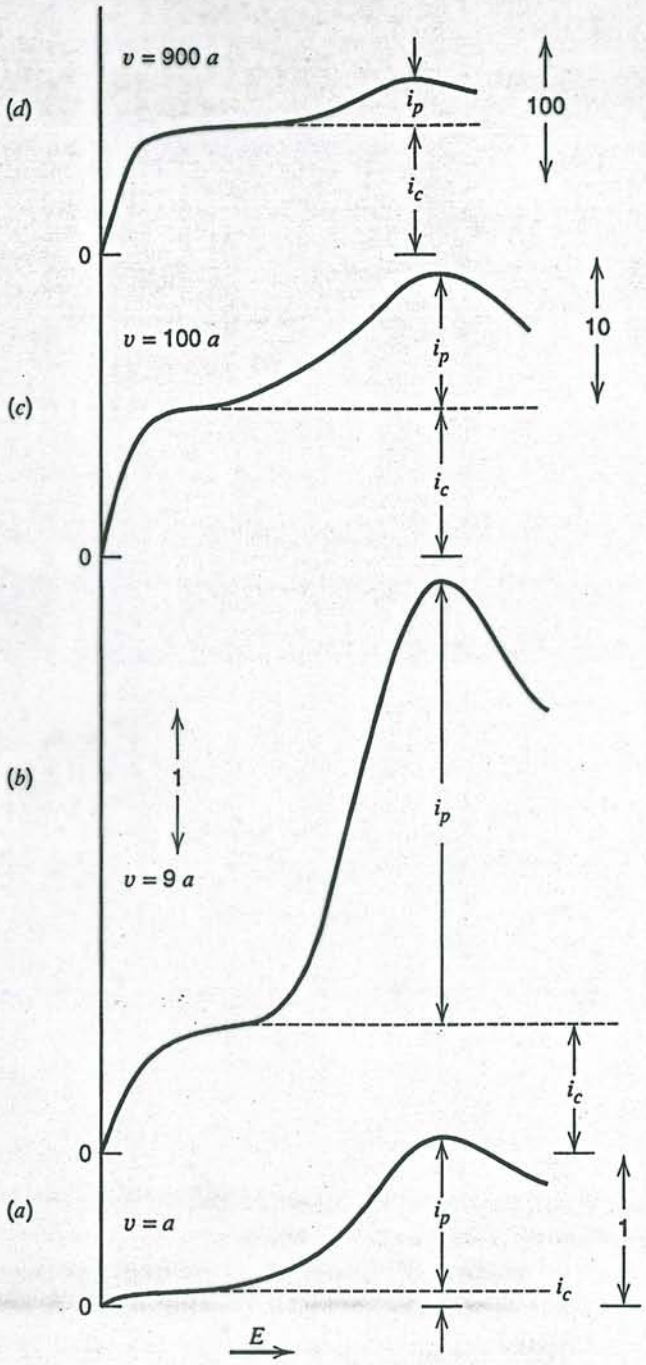

Figure 6.2.3 Effect of double-layer charging at different sweep rates on a linear potential sweep voltammogram. Curves are plotted with the assumption that C_d is independent of E. The magnitudes of the charging current, i_c, and the faradaic peak current, i_p, are shown. Note that the current scale in (*c*) is 10× and in (*d*) is 100× that in (*a*) and (*b*).

An important practical limitation of very fast voltammetry [other than instrumental and R_u and C_d considerations (11)], is the importance of adsorption of even small amounts of electroactive substance or faradaic changes involving the electrode surface (e.g., formation of an oxide layer). As shown in Section 14.3, for surface processes like double-layer charging, the current response varies directly with v. Therefore, surface effects of minor importance at small v can dominate at high scan rates.

6.3 TOTALLY IRREVERSIBLE SYSTEMS

6.3.1 The Boundary Value Problem

For a totally irreversible one-step, one-electron reaction ($O + e \xrightarrow{k_f} R$) the nernstian boundary condition, (6.2.2), is replaced by (see Section 5.5)

$$\frac{i}{nFA} = D_O\left[\frac{\partial C_O(x,t)}{\partial x}\right]_{x=0} = k_f(t)C_O(0,t) \qquad (6.3.1)$$

where

$$k_f(t) = k^0 \exp\{-\alpha f[E(t) - E^{0'}]\} \tag{6.3.2}$$

Introducing $E(t)$ from (6.2.1) into (6.3.2) yields

$$k_f(t)C_O(0, t) = k_{fi}C_O(0, t)e^{bt} \tag{6.3.3}$$

where $b = \alpha f v$ and

$$k_{fi} = k^0 \exp[-\alpha f(E_i - E^{0'})] \tag{6.3.4}$$

The solution follows in an analogous manner to that described in Section 6.2.1 and again requires a numerical solution of an integral equation (3, 5). The current is given by

$$i = FAC_O^*(\pi D_O b)^{1/2}\chi(bt) \tag{6.3.5}$$

$$i = FAC_O^* D_O^{1/2} v^{1/2} \left(\frac{\alpha F}{RT}\right)^{1/2} \pi^{1/2}\chi(bt) \tag{6.3.6}$$

where $\chi(bt)$ is a function [different from $\chi(\sigma t)$] tabulated in Table 6.3.1. Again, i at any point on the wave varies with $v^{1/2}$ and C_O^*.

For spherical electrodes, a procedure analogous to that employed at planar electrodes has been proposed. Table 6.3.1 contains values of the spherical correction factor, $\phi(bt)$ employed in the equation

$$i = i(\text{plane}) + \frac{FAD_O C_O^* \phi(bt)}{r_0} \tag{6.3.7}$$

TABLE 6.3.1 Current Functions for Irreversible Charge Transfer (3)[a]

Dimensionless Potential[b]	Potential[c] mV at 25°C	$\pi^{1/2}\chi(bt)$	$\phi(bt)$	Dimensionless Potential[b]	Potential[c] mV at 25°C	$\pi^{1/2}\chi(bt)$	$\phi(bt)$
6.23	160	0.003		0.58	15	0.437	0.323
5.45	140	0.008		0.39	10	0.462	0.396
4.67	120	0.016		0.19	5	0.480	0.482
4.28	110	0.024		0.00	0	0.492	0.600
3.89	100	0.035		−0.19	−5	0.496	0.685
3.50	90	0.050		−0.21	−5.34	0.4958	0.694
3.11	80	0.073	0.004	−0.39	−10	0.493	0.755
2.72	70	0.104	0.010	−0.58	−15	0.485	0.823
2.34	60	0.145	0.021	−0.78	−20	0.472	0.895
1.95	50	0.199	0.042	−0.97	−25	0.457	0.952
1.56	40	0.264	0.083	−1.17	−30	0.441	0.992
1.36	35	0.300	0.115	−1.36	−35	0.423	1.000
1.17	30	0.337	0.154	−1.56	−40	0.406	
0.97	25	0.372	0.199	−1.95	−50	0.374	
0.78	20	0.406	0.253	−2.72	−70	0.323	

[a]To calculate the current:

1. $i = i(\text{plane}) + i(\text{spherical correction})$.
2. $i = FAD_O^{1/2}C_O^* b^{1/2}\pi^{1/2}\chi(bt) + FAD_O C_O^*(1/r_0)\phi(bt)$
3. $i = 602AD_O^{1/2}C_O^*\alpha^{1/2}v^{1/2}\{\pi^{1/2}\chi(bt) + 0.160[D_O^{1/2}/(r_0\alpha^{1/2}v^{1/2})]\phi(bt)\}$. Units for step 3 are the same as in Table 6.2.1.

[b]Dimensionless potential is $(\alpha F/RT)(E - E^{0'}) + \ln[(\pi D_O b)^{1/2}/k^0]$.

[c]Potential scale in mV for 25°C is $\alpha(E - E^{0'}) + (59.1)\ln[(\pi D_O b)^{1/2}/k^0]$.

6.3.2 Peak Current and Potential

The function $\chi(bt)$ goes through a maximum at $\pi^{1/2}\chi(bt) = 0.4958$. Introduction of this value into (6.3.6) yields the following for the peak current:

$$i_p = (2.99 \times 10^5)\alpha^{1/2} A C_O^* D_O^{1/2} v^{1/2} \tag{6.3.8}$$

where the units are as for (6.2.19). From Table 6.3.1, the peak potential, E_p, is given by

$$\alpha(E_p - E^{0'}) + \frac{RT}{F}\ln\left[\frac{(\pi D_O b)^{1/2}}{k^0}\right] = -0.21\frac{RT}{F} = -5.34 \text{ mV at } 25°C \tag{6.3.9}$$

or

$$E_p = E^{0'} - \frac{RT}{\alpha F}\left[0.780 + \ln\left(\frac{D_O^{1/2}}{k^0}\right) + \ln\left(\frac{\alpha F v}{RT}\right)^{1/2}\right] \tag{6.3.10}$$

$$|E_p - E_{p/2}| = \frac{1.857RT}{\alpha F} = \frac{47.7}{\alpha} \text{ mV at } 25°C \tag{6.3.11}$$

where $E_{p/2}$ is the potential where the current is at half the peak value. For a totally irreversible wave, E_p is a function of scan rate, shifting (for a reduction) in a negative direction by an amount $1.15RT/\alpha F$ (or $30/\alpha$ mV at 25°C) for each tenfold increase in v. Also, E_p occurs *beyond* $E^{0'}$ (i.e., more negative for a reduction) by an activation overpotential related to k^0. An alternative expression for i_p in terms of E_p can be obtained by combining (6.3.10) with (6.3.6), so that the result contains the value of $\chi(bt)$ at the peak. After rearrangement and evaluation of the constants, the following equation is obtained (3, 6):

$$i_p = 0.227\, FAC_O^* k^0 \exp[-\alpha f(E_p - E^{0'})] \tag{6.3.12}$$

A plot of $\ln i_p$ *vs.* $E_p - E^{0'}$ (assuming $E^{0'}$ can be obtained) determined at different scan rates should have a slope of $-\alpha f$ and an intercept proportional to k^0.

For an irreversible process more complicated than the one-step, one-electron reaction, it is usually not feasible to derive equations describing the current-potential relationship. In the general case, the more practical approach is to compare experimental behavior with the predictions from simulations (see Appendix B and Chapter 12). Analytical equations may be achievable for a few of the simpler possibilities (see Section 3.5.4). The most important is an overall n-electron process having an irreversible heterogeneous one-electron transfer as the rate-controlling first step. In that case, all equations describing currents in this section [(6.3.5)–(6.3.8), (6.3.12), and in the notes to Table 6.3.1] apply, but with the right hand side multiplied by n. The equations describing potentials [(6.3.9)–(6.3.11)] apply without alteration.

6.4 QUASIREVERSIBLE SYSTEMS

Matsuda and Ayabe (5) coined the term *quasireversible* for reactions that show electron-transfer kinetic limitations where the reverse reaction has to be considered, and they provided the first treatment of such systems. For the one-step, one-electron case,

$$O + e \underset{k_b}{\overset{k_f}{\rightleftarrows}} R \tag{6.4.1}$$

the corresponding boundary condition is [from (5.5.3)]

$$D_O\left(\frac{\partial C_O(x,t)}{\partial x}\right)_{x=0} = k^0 e^{-\alpha f[E(t)-E^{0'}]}\{C_O(0,t) - C_R(0,t)e^{f[E(t)-E^{0'}]}\} \tag{6.4.2}$$

The shape of the peak and the various peak parameters were shown to be functions of α and a parameter Λ, defined as

$$\Lambda = \frac{k^0}{(D_O^{1-\alpha} D_R^{\alpha} f v)^{1/2}} \tag{6.4.3}$$

or, for $D_O = D_R = D$,

$$\Lambda = \frac{k^0}{(Dfv)^{1/2}} \tag{6.4.4}$$

The current is given by

$$i = FAD_O^{1/2} C_O^* f^{1/2} v^{1/2} \Psi(E) \tag{6.4.5}$$

where $\Psi(E)$ is shown in Figure 6.4.1. Note that when $\Lambda > 10$, the behavior approaches that of a reversible system.

The values of i_p, E_p, and $E_{p/2}$ depend on Λ and α. The peak current is given by

$$i_p = i_p(\text{rev}) K(\Lambda, \alpha) \tag{6.4.6}$$

where i_p(rev) is the reversible i_p value (equation 6.2.18), and the function $K(\Lambda, \alpha)$ is shown in Figure 6.4.2. Note that for a quasireversible reaction, i_p is not proportional to $v^{1/2}$.

The peak potential is

$$E_p - E_{1/2} = -\Xi(\Lambda, \alpha)\left(\frac{RT}{F}\right) = -26\Xi(\Lambda, \alpha) \text{ mV at } 25°\text{C} \tag{6.4.7}$$

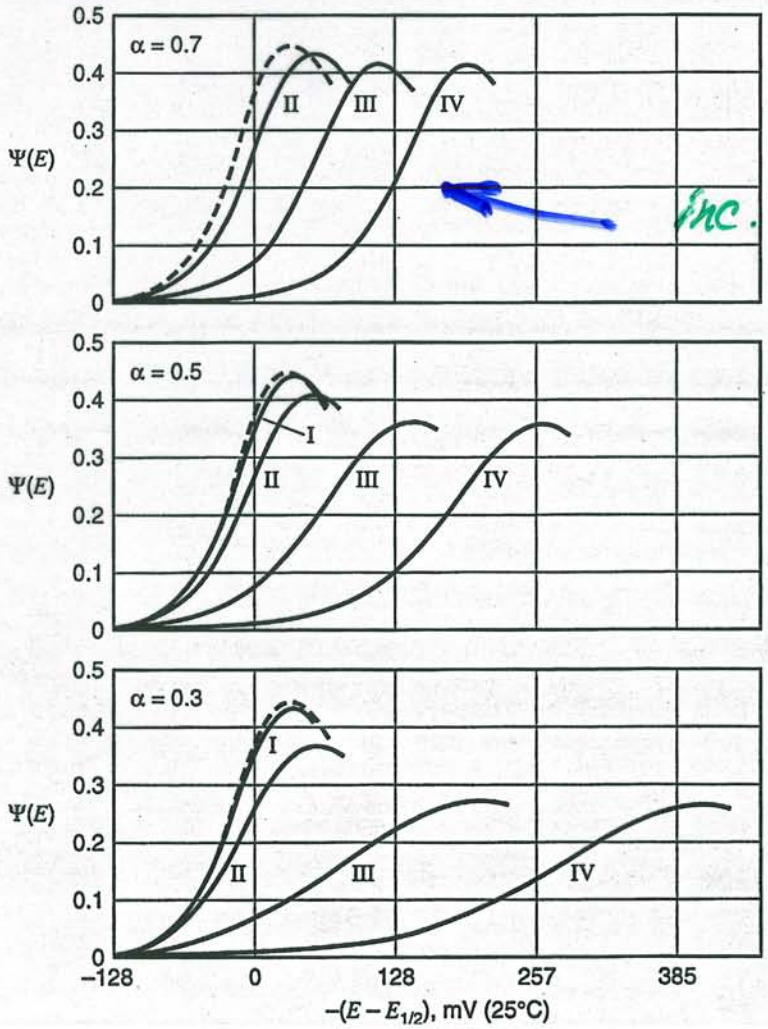

Figure 6.4.1 Variation of quasireversible current function, $\Psi(E)$, for different values of α (as indicated on each graph) and the following values of Λ: (I) $\Lambda = 10$;(II) $\Lambda = 1$; (III) $\Lambda = 0.1$; (IV) $\Lambda = 10^{-2}$. Dashed curve is for a reversible reaction. $\Psi(E) = i/FAC_O^* D_O^{1/2} (nF/RT)^{1/2} v^{1/2}$ and $\Lambda = k^0/[D^{1/2}(F/RT)^{1/2} v^{1/2}]$ (for $D_O = D_R = D$). [From H. Matsuda and Y. Ayabe, *Z. Elektrochem.*, **59**, 494 (1955), with permission. Abscissa label adapted for this text.]

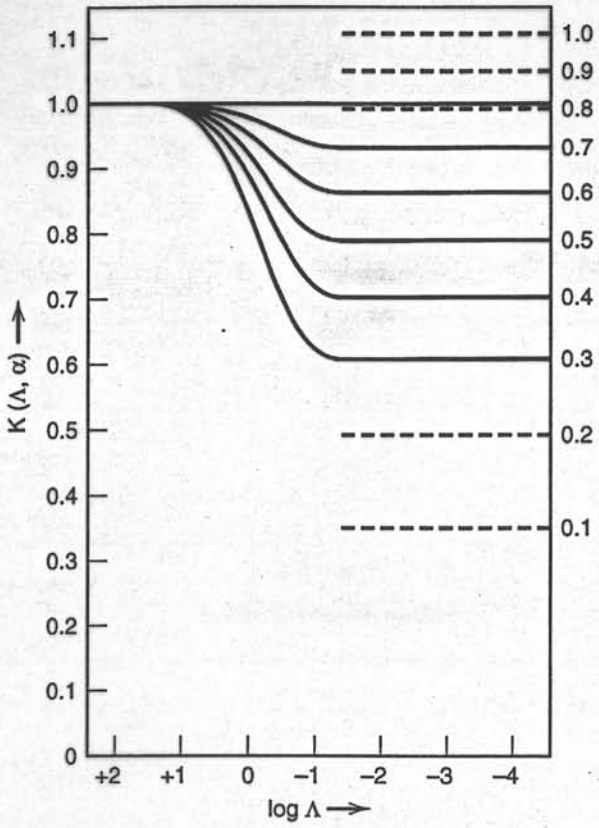

Figure 6.4.2 Variation of $K(\Lambda, \alpha)$ with Λ for different values of α. Dashed lines show functions for a totally irreversible reaction. $K(\Lambda, \alpha) = i_p/i_p(\text{rev})$. [From H. Matsuda and Y. Ayabe, *Z. Elektrochem.*, **59**, 494 (1955), with permission.]

where $\Xi(\Lambda, \alpha)$ is shown in Figure 6.4.3. For the half-peak potential, we have

$$E_{p/2} - E_p = \Delta(\Lambda, \alpha)\left(\frac{RT}{F}\right) = 26\Delta(\Lambda, \alpha) \text{ mV at } 25°\text{C} \tag{6.4.8}$$

where $\Delta(\Lambda, \alpha)$ is given in Figure 6.4.4.

The parameters $K(\Lambda, \alpha)$, $\Xi(\Lambda, \alpha)$, and $\Delta(\Lambda, \alpha)$ attain limiting values characteristic of reversible or totally irreversible processes as Λ varies. For example, consider $\Delta(\Lambda, \alpha)$. For $\Lambda \geq 10$, $\Delta(\Lambda, \alpha) \approx 2.2$, yielding the $E_p - E_{p/2}$ value characteristic of a reversible wave, (6.2.22). For $\Lambda < 10^{-2}$ and $\alpha = 0.5$, $\Delta(\Lambda, \alpha) \approx 3.7$, yielding the totally irreversible charac-

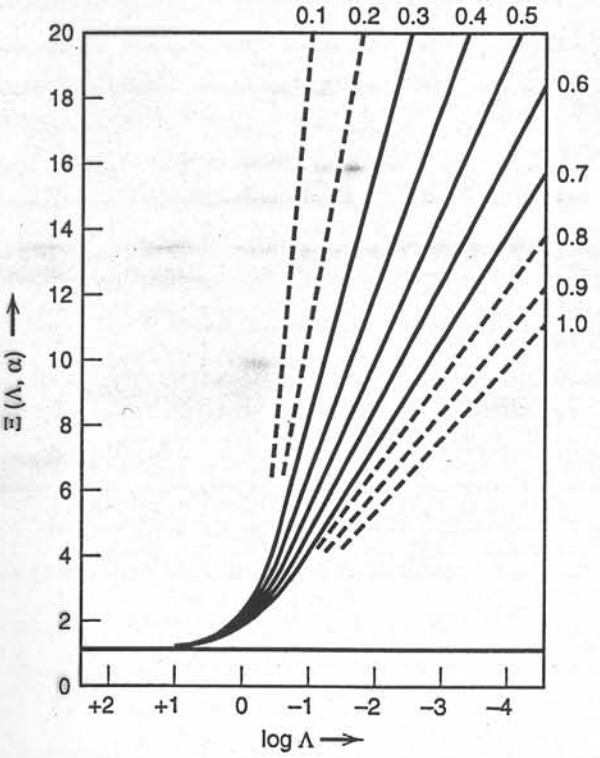

Figure 6.4.3 Variation of $\Xi(\Lambda, \alpha)$ with Λ for different values of α. Dashed lines show functions for a totally irreversible reaction. $\Xi(\Lambda, \alpha) = -(E_p - E_{1/2})F/RT$. [From H. Matsuda and Y. Ayabe, *Z. Elektrochem.*, **59**, 494 (1955), with permission.]

in Sweep voltammetry, why does $i(E)$ go through a maximum and not reach a plateau at i_{lim}?

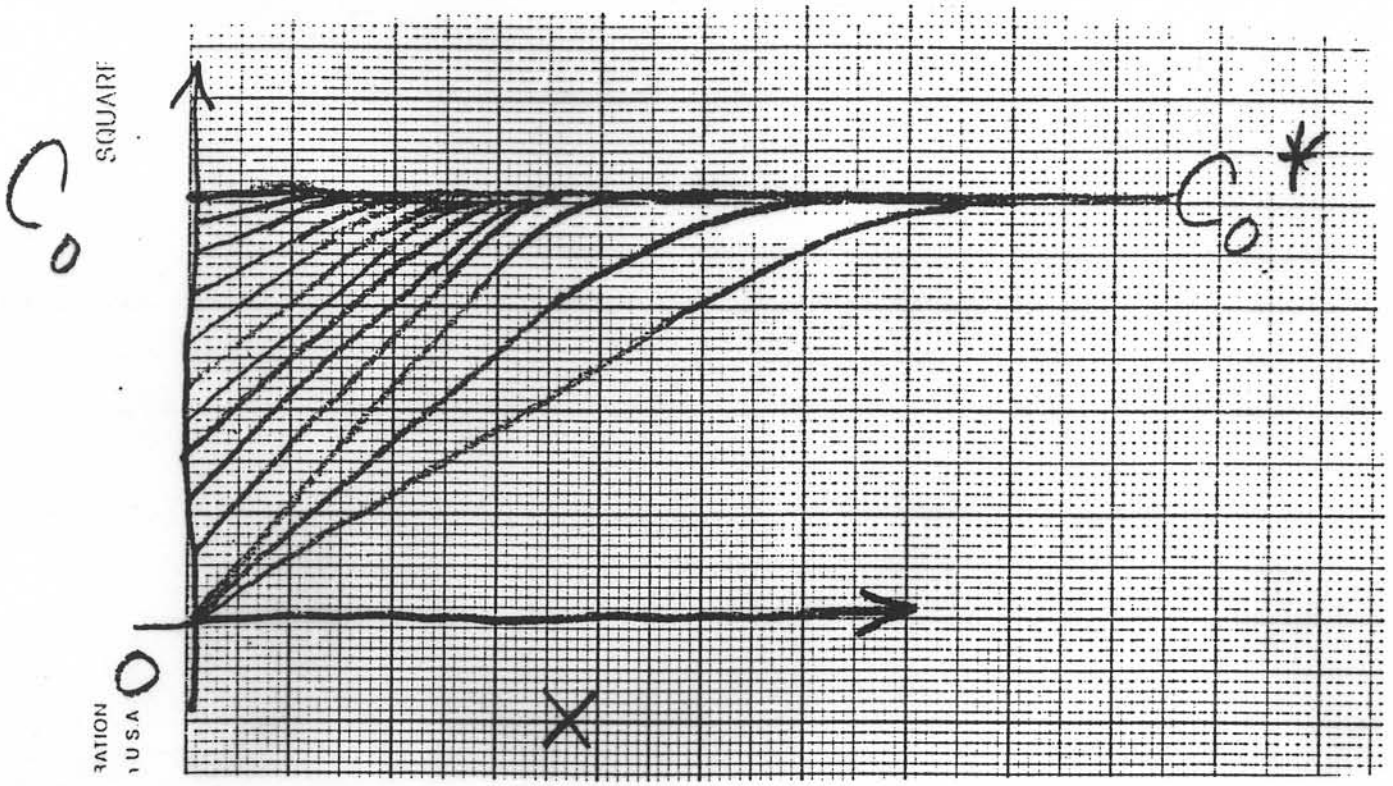

$\Rightarrow i \propto \left(\frac{\partial C_O}{\partial X}\right)_{X=0}$ and $\left(\frac{\partial C_O}{\partial X}\right)_{X=0}$ goes through a maximum

$\Rightarrow i_p$ occurs when $\left(\frac{\partial C_O}{\partial X}\right)_{X=0}$ takes max. value

which most likely occurs when $C_O = 0$

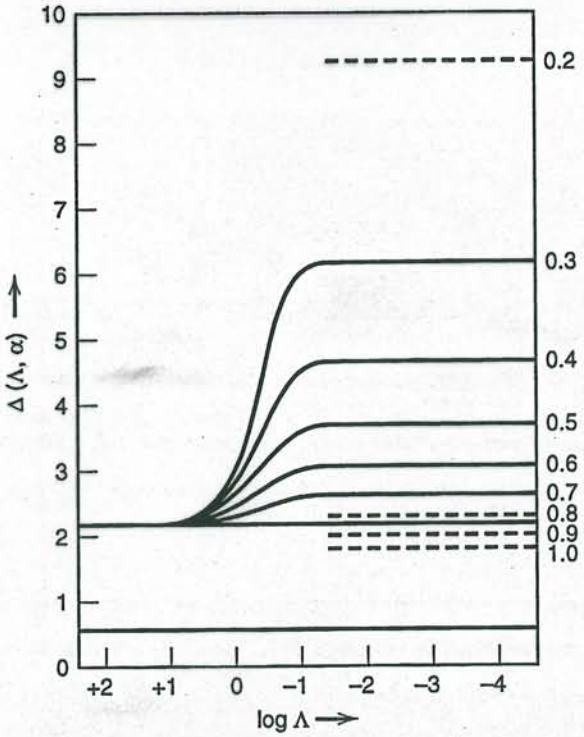

Figure 6.4.4 Variation of $\Delta(\Lambda, \alpha)$ with Λ and α. Dashed lines show functions for a totally irreversible reaction. $\Delta(\Lambda, \alpha) = (E_{p/2} - E_p)F/RT$. [From H. Matsuda and Y. Ayabe, *Z. Elektrochem.*, **59**, 494 (1955), with permission.]

teristic, (6.3.11). Thus a system may show nernstian, quasireversible, or totally irreversible behavior, depending on Λ, or experimentally, on the scan rate employed. The appearance of kinetic effects depends on the time window of the experiment, which is essentially the time needed to traverse the LSV wave (see Chapter 12). At small v (or long times), systems may yield reversible waves, while at large v (or short times), irreversible behavior is observed. In Section 5.5, we reached the same conclusions in the context of potential step experiments. Matsuda and Ayabe (5) suggested the following zone boundaries for LSV:[6]

Reversible (nernstian)	$\Lambda \geq 15$; $k^0 \geq 0.3v^{1/2}$ cm/s
Quasireversible	$15 \geq \Lambda \geq 10^{-2(1+\alpha)}$; $0.3v^{1/2} \geq k^0 \geq 2 \times 10^{-5}\, v^{1/2}$ cm/s
Totally irreversible	$\Lambda \leq 10^{-2(1+\alpha)}$; $k^0 \leq 2 \times 10^{-5}\, v^{1/2}$ cm/s

6.5 CYCLIC VOLTAMMETRY

The reversal experiment in linear scan voltammetry is carried out by switching the direction of the scan at a certain time, $t = \lambda$ (or at the *switching potential*, E_λ). Thus the potential is given at any time by

$$(0 < t \leq \lambda) \qquad E = E_i - vt \tag{6.5.1}$$

$$(t > \lambda) \qquad E = E_i - 2v\lambda + vt \tag{6.5.2}$$

While it is possible to use a different scan rate (v') on reversal (12), this is rarely done, and only the case of a symmetrical triangular wave is considered here. The theoretical treatment follows that of Section 6.2, except that (6.5.2) is used in the concentration-potential equation, rather than (6.2.1), for $t > \lambda$. This sweep reversal method, called *cyclic voltammetry*, is extremely powerful and is among the most widely practiced of all electrochemical methods.

6.5.1 Nernstian Systems

Application of (6.5.2) in the equation for a nernstian system, (5.4.6), yields (6.2.3), where $S(t)$is now given by

$$(t > \lambda) \qquad S(t) = e^{\sigma t - 2\sigma\lambda} \tag{6.5.3}$$

[6]The k^0 values are based on $n = 1$, $\alpha = 0.5$, $T = 25°C$, and $D = 10^{-5}$ cm^2/s. With v in V/s, $\Lambda \approx k^0/(39Dv)^{1/2}$.

The derivation then proceeds as in Section 6.2. The shape of the curve on reversal depends on the switching potential, E_λ, or how far beyond the cathodic peak the scan is allowed to proceed before reversal. However, if E_λ is at least $35/n$ mV past the cathodic peak,[7] the reversal peaks all have the same general shape, basically consisting of a curve shaped like the forward *i-E* curve plotted in the opposite direction on the current axis, with the decaying current of the cathodic wave used as a baseline. Typical *i-t* curves for different switching potentials are shown in Figure 6.5.1. This type of presentation would result if the curves were recorded on a time base. The more usual *i-E* presentation is shown in Figure 6.5.2.

Two measured parameters of interest on these *i-E* curves (*cyclic voltammograms*) are the ratio of peak currents, i_{pa}/i_{pc}, and the separation of peak potentials, $E_{pa} - E_{pc}$. For a nernstian wave with stable product, $i_{pa}/i_{pc} = 1$ regardless of scan rate, E_λ (for $E_\lambda > 35/n$ mV past E_{pc}), and diffusion coefficients, when i_{pa} is measured from the decaying cathodic current as a baseline (see Figures 6.5.1 and 6.5.2). This baseline can be determined by the methods described in Section 6.6.

If the cathodic sweep is stopped and the current is allowed to decay to zero (Figure 6.5.2, curve 4), the resulting anodic *i-E* curve is identical in shape to the cathodic one, but is plotted in the opposite direction on both the *i* and *E* axes. This is so because allowing the cathodic current to decay to zero results in the diffusion layer being depleted of O and populated with R at a concentration near C_O^*, so that the anodic scan is virtually the same as that which would result from an initial anodic scan in a solution containing only R.

Deviation of the ratio i_{pa}/i_{pc} from unity is indicative of homogeneous kinetic or other complications in the electrode process (13), as discussed in more detail in Chapter 12.

Nicholson (14) suggested that if the actual baseline for measuring i_{pa} cannot be determined, the ratio can be calculated from (a) the uncorrected anodic peak current, $(i_{pa})_0$, with respect to the zero current baseline (see Figure 6.5.2, curve 3) and (b) the current at E_λ, $(i_{sp})_0$, by the expression:

$$\frac{i_{pa}}{i_{pc}} = \frac{(i_{pa})_0}{i_{pc}} + \frac{0.485(i_{sp})_0}{i_{pc}} + 0.086 \qquad (6.5.4)$$

In real cyclic voltammograms the faradaic response is superimposed on an approximately constant charging current. The situation for the forward scan was discussed in Section 6.2.4. Upon reversal, the magnitude of dE/dt remains constant but the sign changes; hence the charging current is also of the same size, but opposite in sign. It forms a baseline for the reversal response just as for the forward scan, and both i_{pc} and i_{pa} must be corrected correspondingly.

The measurement of peak currents in CV is imprecise because the correction for charging current is typically uncertain. For the reversal peak, the imprecision is increased further because one cannot readily define the folded faradaic response for the forward process (e.g., curve 1′, 2′, or 3′ in Figure 6.5.2) to use as a reference for the measurement. Consequently, CV is not an ideal method for quantitative evaluation of system properties that must be derived from peak heights, such as the concentration of an electroactive species or the rate constant of a coupled homogeneous reaction. The method's power lies in its diagnostic strength, which is derived from the ease of interpreting qualitative and semi-quantitative behavior. Once a system is understood mechanistically, other methods are often better suited for the precise evaluation of parameters.

[7]This condition is based on the assumption that the potentiostat responds ideally and that the effects of R_u are negligible (see Section 1.2.4). A larger margin between the peak and the switching potential would be needed in less ideal circumstances.

Table 6.5.1 Variation of ΔE_p with E_λ for a Nernstian System at 25°C (3)

$n(E_{pc} - E_\lambda)$ (mV)	$n(E_{pa} - E_{pc})$ (mV)
71.5	60.5
121.5	59.2
171.5	58.3
271.5	57.8
∞	57.0

6.5.2 Quasireversible Reactions

By using the potential program given by (6.5.1) and (6.5.2) in the equations for linear scan voltammetry in Section 6.4, the *i-E* curves for the quasireversible one-step, one-electron process can be derived. In this case the wave shape and ΔE_p are functions of v, k^0, α, and E_λ. As before, however, if E_λ is at least $90/n$ mV beyond the cathodic peak, the effect of E_λ is small. In this case the curves are functions of the dimensionless parameters α and either Λ (see equation 6.4.3) or an equivalent parameter, ψ defined by[8]

$$\psi = \Lambda\pi^{-1/2} = \frac{\left(\frac{D_O}{D_R}\right)^{\alpha/2} k^0}{(\pi D_O f v)^{1/2}} \tag{6.5.5}$$

Typical behavior is shown in Figure 6.5.3.

For $0.3 < \alpha < 0.7$ the ΔE_p values are nearly independent of α and depend only on ψ. Table 6.5.2, which provides data linking ψ to k^0 in this range (14), is the basis for a widely used method (often called the *method of Nicholson*) for estimating k^0 in quasireversible

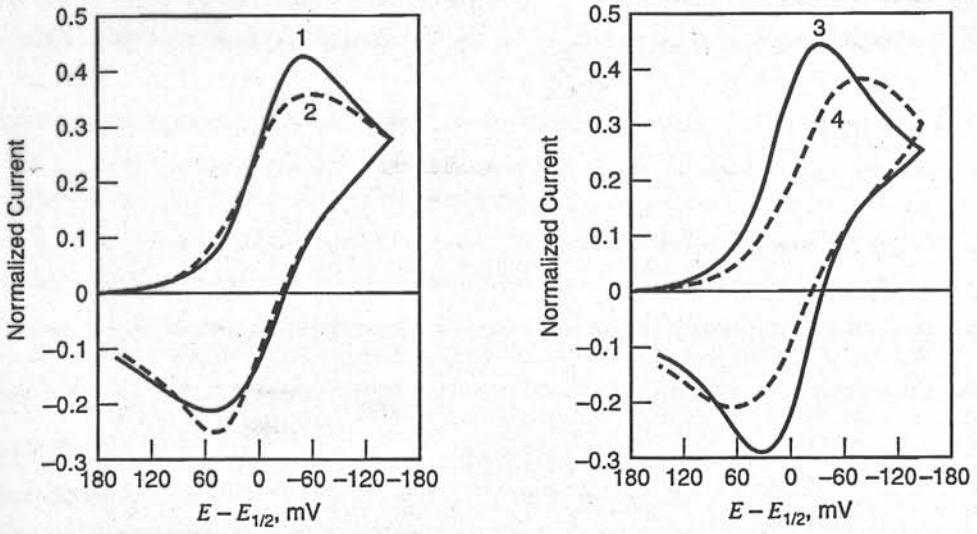

Figure 6.5.3 Theoretical cyclic voltammograms showing effect of ψ and α on curve shape for a one-step, one-electron reaction. Curve 1: $\psi = 0.5$, $\alpha = 0.7$. Curve 2: $\psi = 0.5$, $\alpha = 0.3$. Curve 3: $\psi = 7.0$, $\alpha = 0.5$. Curve 4: $\psi = 0.25$, $\alpha = 0.5$. [Reproduced with permission from R. S. Nicholson, *Anal. Chem.*, **37**, 1351 (1965). Copyright 1965, American Chemical Society. Abscissa label adapted for this text.]

[8]Note that ψ in (6.5.5) is not the same as $\Psi(E)$ in (6.4.5).

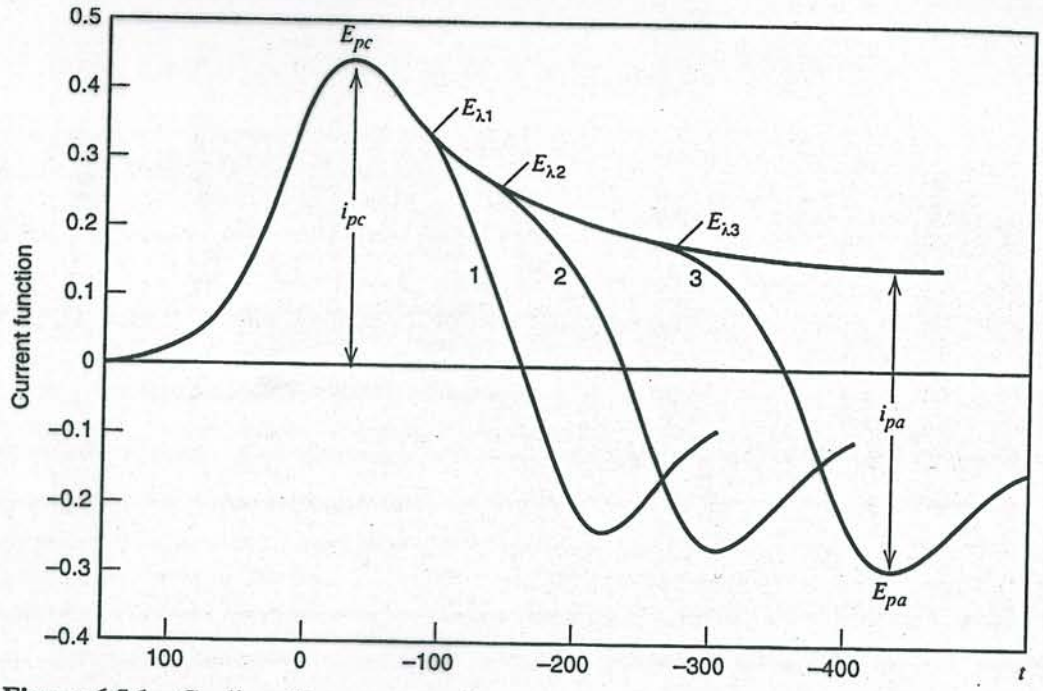

Figure 6.5.1 Cyclic voltammograms for reversal at different E_λ values, with presentation on a time base.

The difference between E_{pa} and E_{pc}, often symbolized by ΔE_p, is a useful diagnostic test of a nernstian reaction. Although ΔE_p is slightly a function of E_λ, it is always close to $2.3RT/nF$ (or $59/n$ mV at 25°C). Actual values as a function of E_λ are shown in Table 6.5.1. For repeated cycling the cathodic peak current decreases and the anodic one increases until a steady-state pattern is attained. At steady state $\Delta E_p = 58/n$ mV at 25°C (5).

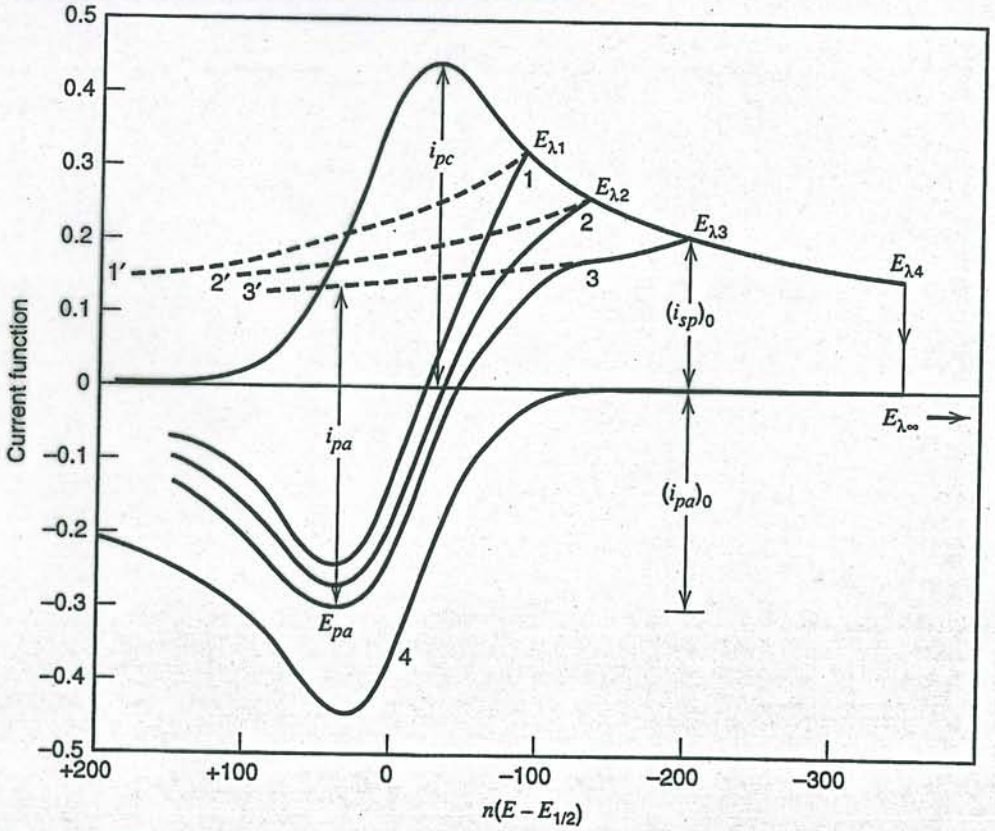

Figure 6.5.2 Cyclic voltammograms under the same conditions as in Figure 6.5.1, but in an *i-E* format. E_λ of (*1*) $E_{1/2} - 90/n$; (*2*) $E_{1/2} - 130/n$; (*3*) $E_{1/2} - 200/n$ mV; (*4*) for potential held at $E_{\lambda 4}$ until the cathodic current decays to zero. [Curve 4 results from reflection of the cathodic *i-E* curve through the *E* axis and then through the vertical line at $n(E - E_{1/2}) = 0$. Curves 1, 2, and 3 result by addition of this curve to the decaying current of the cathodic *i-E* curve (1′, 2′, or 3′).]

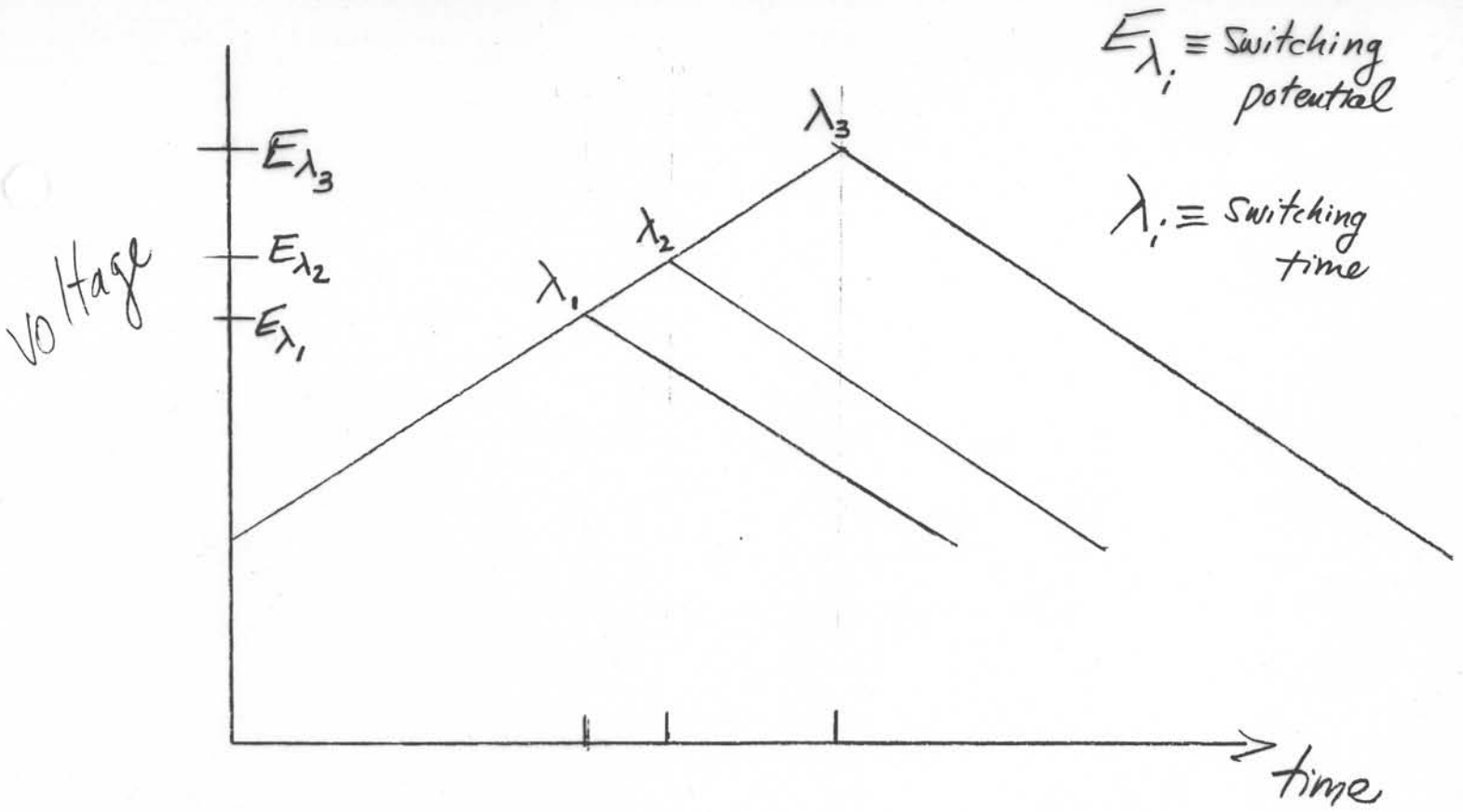

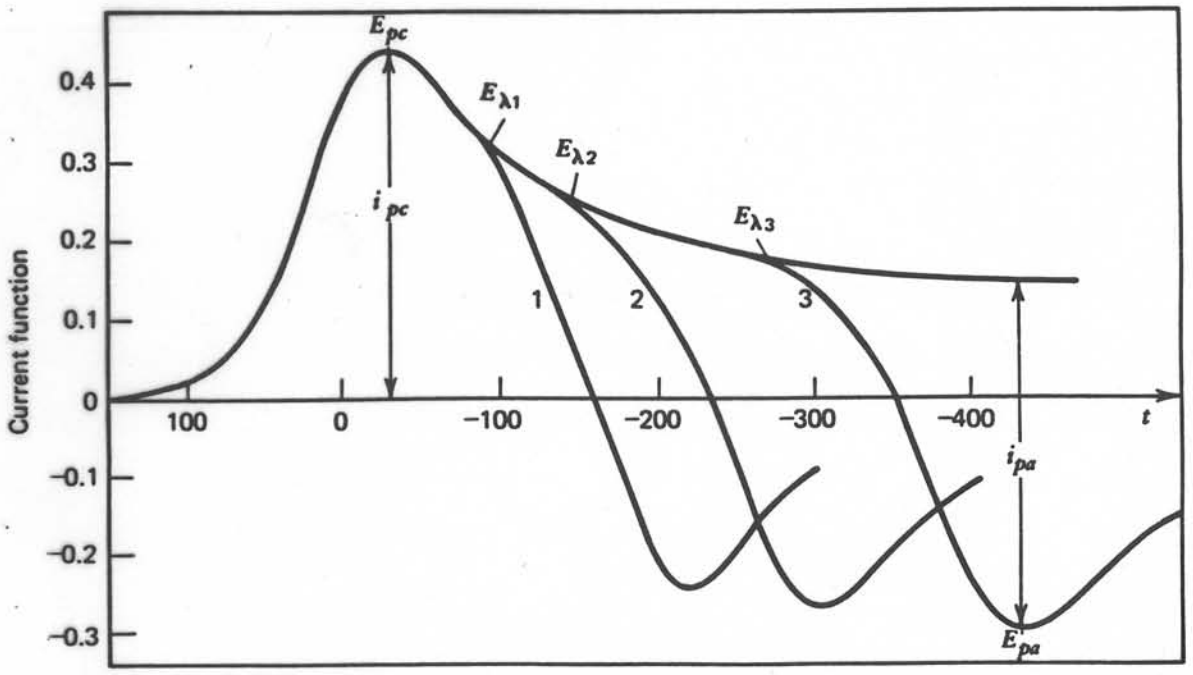

Figure 6.5.1
Cyclic voltammograms for reversal at different E_λ values with presentations as they appear on a strip-chart recorder (i-t curves).

Table 6.5.2 Variation of ΔE_p with ψ at 25°C (14)[a]

ψ	$E_{pa} - E_{pc}$ mV
20	61
7	63
6	64
5	65
4	66
3	68
2	72
1	84
0.75	92
0.50	105
0.35	121
0.25	141
0.10	212

[a]For a one-step, one-electron process with $E_\lambda = E_p - 112.5/n$ mV and $\alpha = 0.5$.

systems. One determines the variation of ΔE_p with v, and from this variation, ψ. The approach is closely related to the determination of the electron-transfer kinetics by the shift of E_p with v as described in Section 6.4.

With both of these approaches one must be sure that the uncompensated resistance, R_u, is sufficiently small that the resulting voltage drops (of the order of $i_p R_u$) are negligible compared to the ΔE_p attributable to kinetic effects. In fact, Nicholson (14) has shown that resistive effects cannot be readily detected in the ΔE_p-v plot, because the effect of uncompensated resistance on the ΔE_p-v behavior is almost the same as that of ψ. The effect of R_u is most important when the currents are large and when k^0 approaches the reversible limit (so that) ΔE_p differs only slightly from the reversible value). It is especially difficult not to have a few ohms of uncompensated resistance in nonaqueous solvents (such as acetonitrile or tetrahydrofuran), even with positive-feedback circuitry (Chapter 15). Many reported studies made under these conditions have suffered from this problem.

▶ 6.6 MULTICOMPONENT SYSTEMS AND MULTISTEP CHARGE TRANSFERS

The consecutive reduction of two substances O and O′ in a potential scan experiment is more complicated than in the potential step (or sampled-current voltammetric) experiment treated in Section 5.6 (15, 16). As before, we consider that the reactions $O + ne \rightarrow R$ and $O' + n'e \rightarrow R'$ occur. If the diffusion of O and O′ takes place independently, the fluxes are additive and the *i-E* curve for the mixture is the sum of the individual *i-E* curves of O and O′ (Figure 6.6.1). Note, however, that the measurement of i'_p must be made using the decaying current of the first wave as the baseline. Usually this baseline is obtained by assuming that the current past the peak potential follows that for the large-amplitude potential step and decays as $t^{-1/2}$. A better fit based on an equation with two adjustable parameters

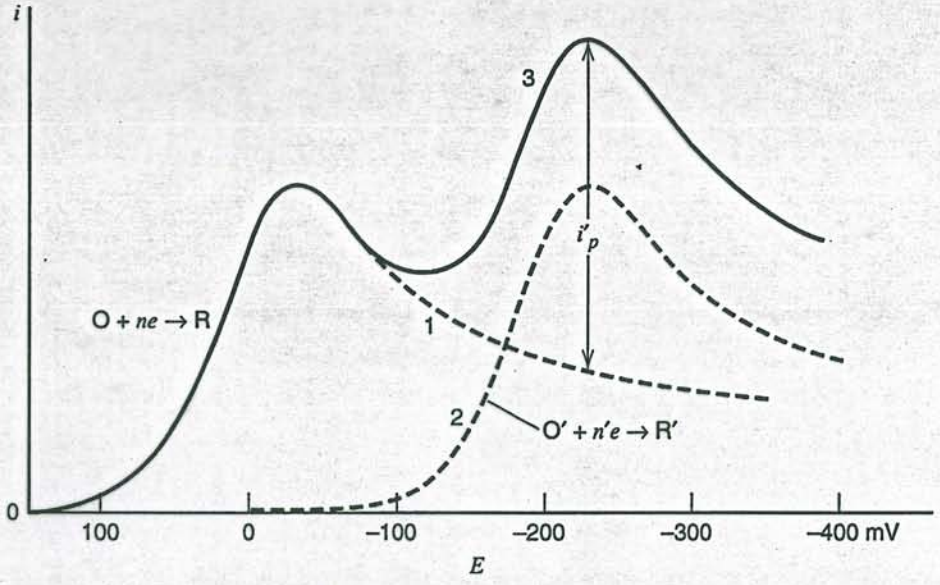

Figure 6.6.1 Voltammograms for solutions of (*1*) O alone; (*2*) O′ alone and, (*3*) mixture of O and O′, with $n = n'$, $C_O^* = C_{O'}^*$, and $D_O = D_{O'}$.

has been suggested by Polcyn and Shain (16); since this fitting procedure depends on the reversibility of the reactions and is a little messy, it is rarely used.

An experimental approach to obtaining the baseline was suggested by Reinmuth (unpublished). Since the concentration of O at the electrode falls essentially to zero at potentials just beyond E_p, the current beyond E_p is independent of potential. Thus if the voltammogram of a single-component system is recorded on a time base (rather than in an X-Y format) and the potential scan is held at about $60/n$ mV beyond E_p while the time base continues, the current-time curve that results will be the same as that obtained with the potential sweep continuing (until a new wave or background reduction occurs). For a two-component system this technique allows establishing the baseline for the second

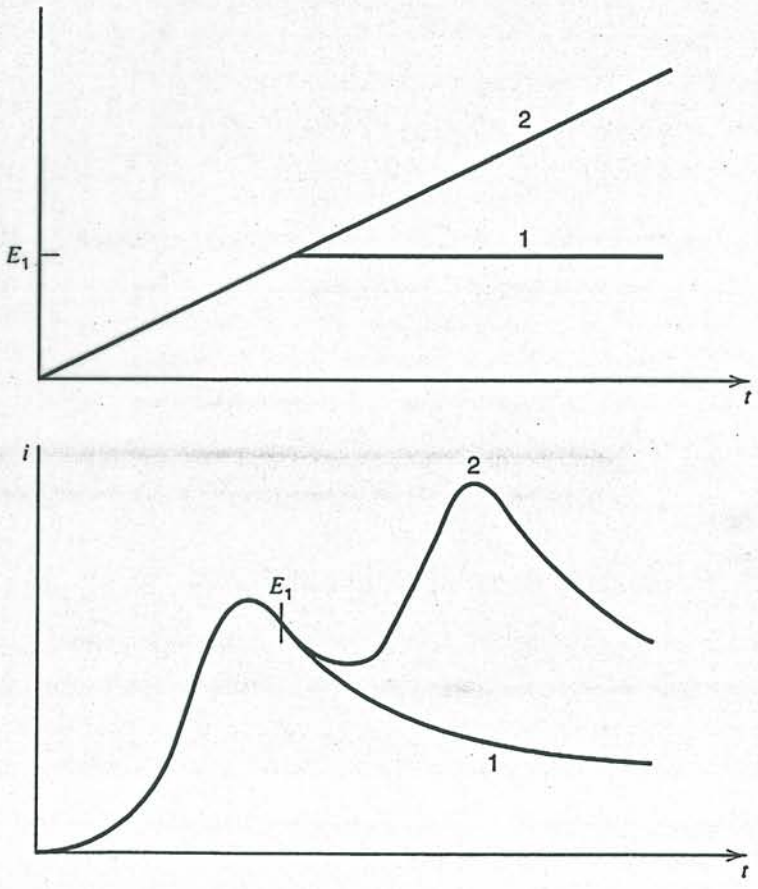

Figure 6.6.2 Method for obtaining baseline for measurement of i'_p of second wave. *Upper curves:* potential programs. *Lower curves:* resulting voltammograms with (curve 1) potential stopped at E_1 and (curve 2) potential scan continued. System as in Figure 6.6.1.

wave by halting the scan somewhere before the foot of the second wave and recording the i-t curve, and then repeating the experiment (after stirring the solution and allowing it to come to rest to reestablish the initial conditions). The second run is made at the same rate and continues beyond the second peak (Figure 6.6.2).

An alternative experimental approach involves stopping the sweep beyond E_p, as before, and allowing the current to decay to a small value (so that O is depleted in the vicinity of the electrode or the concentration gradient of O is essentially zero near the electrode). Then one continues the scan and measures i'_p from the potential axis as a baseline (Figure 6.6.3). The application of this method requires convection-free conditions (quiet, vibration-free solutions, and shielded electrodes oriented to prevent convection from density gradients; see Section 8.3.5), because the waiting time for the current decay must be 20 to 50 times the time needed to traverse a peak.

For the stepwise reduction of a single substance O, that is, $O + n_1e \rightarrow R_1$ (E_1^0), $R_1 + n_2e \rightarrow R_2$ (E_2^0), the situation is similar to the two-component case, but more complicated. If E_1^0 and E_2^0 are well separated, with $E_1^0 > E_2^0$ (i.e., O reduces before R_1), then two separate waves are observed. The first wave corresponds to reduction of O to R_1 in an n_1-electron reaction, with R_1 diffusing into the solution as the wave is traversed. At the second wave, O continues to be reduced, either directly at the electrode or by reaction with R_2 diffusing away from the electrode ($O_1 + R_2 \rightarrow 2R_1$), in an overall ($n_1 + n_2$)-electron reaction, and R_1 diffuses back toward the electrode to be reduced in an n_2-electron reaction. The voltammogram for this case resembles that of Figure 6.6.1.

In general the nature of the i-E curve depends on ΔE^0 $(= E_2^0 - E_1^0)$, the reversibility of each step, and n_1 and n_2. Calculated cyclic voltammograms for different values of ΔE^0 in a system with two one-electron steps are shown in Figure 6.6.4. When ΔE^0 is between 0 and -100 mV, the individual waves are merged into a broad wave whose E_p is independent of scan rate. When $\Delta E^0 = 0$, a single peak with a peak current intermediate between those of single-step $1e$ and $2e$ reactions is found, and $E_p - E_{p/2} = 21$ mV. For $\Delta E^0 > 180$ mV (i.e., the second step is easier than the first), a single wave characteristic of a reversible $2e$ reduction ($O + 2e \rightleftarrows R_2$) is observed (i.e., $\Delta E_p = 2.3RT/2F$).

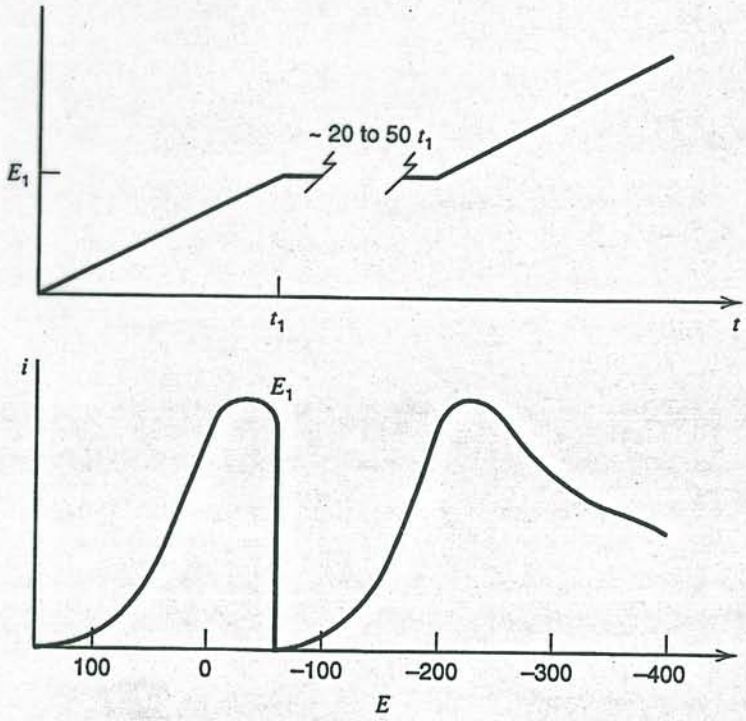

Figure 6.6.3 Method of allowing current of first wave to decay before scanning second wave. *Upper curve:* potential program. *Lower curve:* resulting voltammogram. System as in Figure 6.6.1.

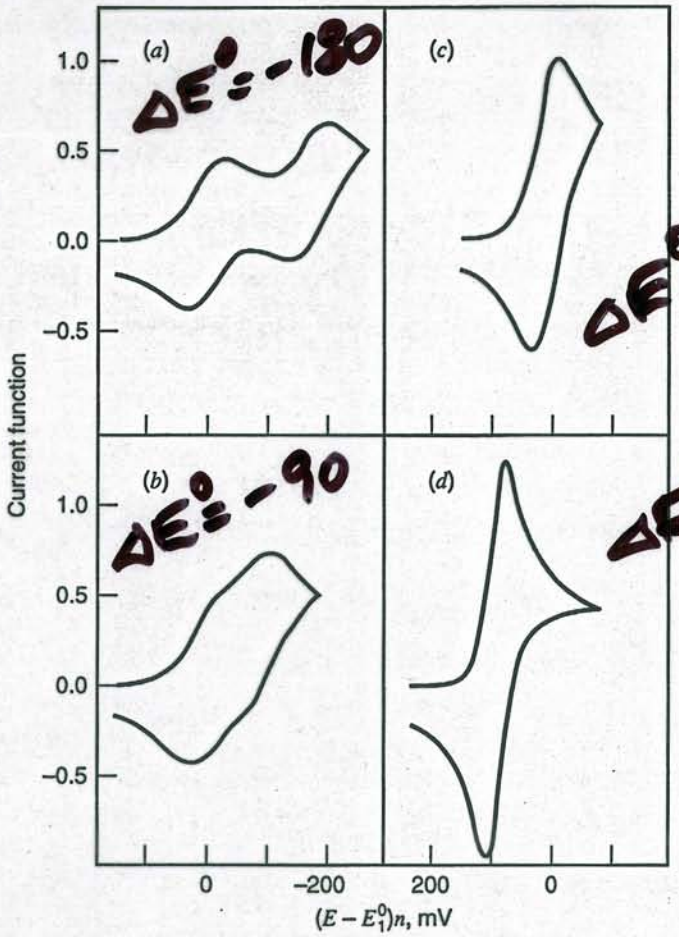

Figure 6.6.4 Cyclic voltammograms for a reversible two-step system at 25°C. Current function is analogous to $\chi(z)$ defined in (6.2.16). $n_2/n_1 = 1.0$. (*a*) $\Delta E^0 = -180$ mV. (*b*) $\Delta E^0 = -90$ mV. (*c*) $\Delta E^0 = 0$ mV. (*d*) $\Delta E^0 = 180$ mV. [Reprinted with permission from D. S. Polcyn and I. Shain, *Anal. Chem.*, **38**, 370 (1966). Copyright 1966, American Chemical Society.]

A case of particular interest occurs when $\Delta E^0 = -(2RT/F) \ln 2 = -35.6$ mV (25°C). This ΔE^0 occurs when there is no interaction between the reducible groups on O, and the additional difficulty in adding the second electron arises purely from statistical (entropic) factors (17). Under these conditions the observed wave has all of the shape characteristics of a one-electron transfer even though it is actually the result of two merged one-electron transfers. This same concept can be extended to the reduction of molecules containing k equivalent, noninteracting, reducible centers (e.g., reducible polymers). For this case the ΔE^0 between the first and kth electron transfers is given by

$$E_k^0 - E_1^0 = -\left(\frac{2RT}{F}\right) \ln k \tag{6.6.1}$$

and again the reduction wave, now involving k merged waves, appears like a single one-electron wave with respect to shape, even though the height corresponds to a k-electron process (18). From these considerations it is clear that for two one-electron transfer reactions, ΔE^0 values more positive than $-(2RT/F) \ln 2$ represent positive interactions (i.e., the second electron transfer is assisted by the first), while ΔE^0 values more negative than $-(2RT/F) \ln 2$ represent negative interactions. Stepwise electron transfers (EE-reactions) are discussed in more detail in Sections 12.3.6 and 12.3.7; see also Polcyn and Shain (16).

Linear sweep and cyclic voltammetric methods have been employed for numerous basic studies of electrochemical systems and for analytical purposes. For example, the technique can be used for *in vivo* monitoring of substances in the kidney or brain (19); a typical example that employed a miniature carbon paste electrode to study ascorbic acid in a rat brain is illustrated in Figure 6.6.5. These techniques are especially powerful tools

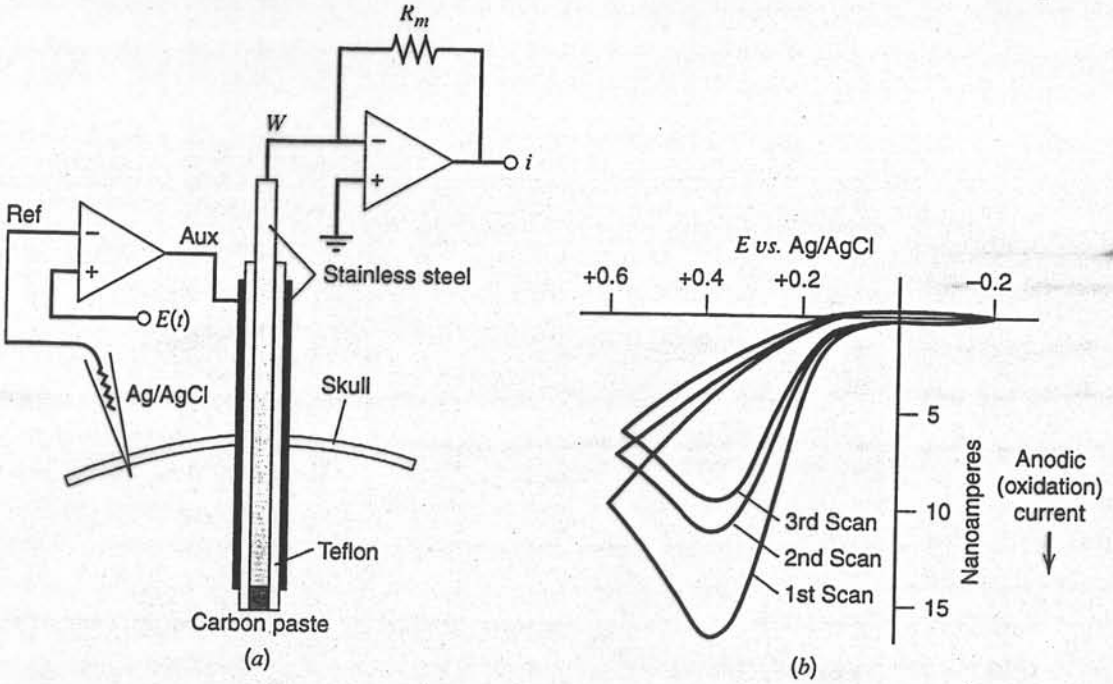

Figure 6.6.5 Application of cyclic voltammetry to *in vivo* analysis in brain tissue. (*a*) Carbon paste working electrode, stainless steel auxiliary electrode (18-gauge cannula), Ag/AgCl reference electrode, and other apparatus for voltammetric measurements. (*b*) Cyclic voltammogram for ascorbic acid oxidation at C-paste electrode positioned in the caudate nucleus of an anesthetized rat. [From P. T. Kissinger, J. B. Hart, and R. N. Adams, *Brain Res.*, **55**, 20 (1973), with permission.]

in the study of electrode reaction mechanisms (Chapter 12) and of adsorbed species (Chapter 14).

▶ 6.7 CONVOLUTIVE OR SEMI-INTEGRAL TECHNIQUES

6.7.1 Principles and Definitions

By proper treatment of the linear potential sweep data, the voltammetric *i*-*E* (or *i*-*t*) curves can be transformed into forms, closely resembling the steady-state voltammetric curves, which are frequently more convenient for further data processing. This transformation makes use of the convolution principle, (A.1.21), and has been facilitated by the availability of digital computers for the processing and acquisition of data. The solution of the diffusion equation for semi-infinite linear diffusion conditions and for species O initially present at a concentration C_O^* yields, for any electrochemical technique, the following expression (see equations 6.2.4 to 6.2.6):

$$C_O(0, t) = C_O^* - \frac{1}{nFAD_O^{1/2}}\left[\frac{1}{\pi^{1/2}}\int_0^t \frac{i(u)}{(t-u)^{1/2}}\,du\right] \tag{6.7.1}$$

If the term in brackets, which represents a particular (convolutive) transformation of the experimental $i(t)$ data, is defined as $I(t)$, then equation 6.7.1 becomes (20)

$$C_O(0, t) = C_O^* - \frac{I(t)}{nFAD_O^{1/2}} \tag{6.7.2}$$

where

$$\boxed{I(t) = \frac{1}{\pi^{1/2}}\int_0^t \frac{i(u)}{(t-u)^{1/2}}\,du} \tag{6.7.3}$$